



Experimental and CFD validation of the thermal performance of a cryogenic batch freezer with the effect of loading

Amisha Chauhan ^a, Jon Trembley ^b, Luiz C. Wrobel ^a, Hussam Jouhara ^{a,*}

^a College of Engineering, Design and Physical Sciences, Brunel University London, Uxbridge, UB8 3PH, UK

^b Air Products PLC, Hersham Place Technology Park, Molesey Road, Surrey, KT12 4RZ, UK

ARTICLE INFO

Article history:

Received 17 September 2018

Received in revised form

14 December 2018

Accepted 19 December 2018

Available online 20 December 2018

Keywords:

CFD

Cryogenic storage

Experimental analysis

Batch freezer

ABSTRACT

Cryogenic freezing systems are used in many industries to preserve food and cell cultures. The freezing methods adopted involve multiple systems to preserve cultures, with many freezing systems using a selection of direct freezing and long-term storage allowing mass and time-efficient freezing methods. However, risks associated with direct freezing using liquid nitrogen can cause cell degradation and crystallisation. This study will focus on the implementation of a batch freezer, using liquid nitrogen sprays to freeze products. The effectiveness of the freezing process will be investigated experimentally for an array of operating conditions. Using numerical methods, additional loading configurations and operation temperatures were also studied to characterise the freezing profile of the system.

© 2018 Elsevier Ltd. All rights reserved.

1. Introduction

The principle of cryogenic preservation can be used in many applications, ranging from food preservation to biological preservation with the use of cryogenic and low temperature systems used to cooling systems; The cryogenic preservation of biological cultures aims to effectively freeze samples with minimal variance in surface temperature, and with minimal changes in biological composition with a focus on energy efficient systems [1–4]. The purpose of this study is to investigate and reflect on the thermal performance on the innovative batch freezer system for the storage of biological substances. The use of effective freezing and storage of biological substances has led to samples such as blood and bone marrow being used years after freezing with minimal changes in their biological composition. However, some issues prevail in food preservation with large variations occurring due to insufficient recirculation zones, lowering the heat transfer coefficient in the area, and the production of ice crystals [5,6]. The production of ice crystals lowers the food quality of produce [7,8], similarly to biological cultures. Conventional studies of the insulative properties of packaging involve the observation of temperature variances [9]. The insulative properties of the air layers existing between the

packaging and product are difficult to determine experimentally. Throughout the application of cryopreservation, a number of pre-treatments have been explored. *Rooni et al.* [10] investigated pre-treatment of lingo-cellulosic materials by using a thermobox and hydrolysis. The study considers a water based pre-treatment to maximise the production of ethanol during fermentation. Similarly, the use of cryogenics has been used in multiple cooling operations such as PV/T cooling [11] and milk chilling units [12,13] with the combination between cryogenics and renewables being investigated.

A large number of CFD simulations exist to study these insulative properties. The majority of studies carried out so far involve the preservation of solid structures and cultures, with success when shafts and porous materials are used. The methods of storing solids are vastly different to that of liquids. The principle of preserving liquids has been observed in the preservation of fruit pulp. *Reno et al.* [14] investigated the storage of liquids using a freezer tunnel, with pulp being contained in metal drums and boxes. The storage containers proved to have effective freezing properties due to the high thermal conductivity of the metal container. Previous studies by *Becker and Fricke* [15] highlighted the significant decrease in heat transfer with the addition of packaging. *Zhao et al.* [16] investigated the effects of packaging through CFD simulations, which were conducted with an air cooling process with the addition of forced convection. The study highlighted the temperature distribution between packaged strawberries with the influence of

* Corresponding author.

E-mail address: hussam.jouhara@brunel.ac.uk (H. Jouhara).

open and closed containers. Further investigations from Alvarez et al. [17] highlighted the influence of product placement and packaging, which can lead to a high variance in temperatures throughout the whole system due to the increased thermal resistance. The study suggests the addition of vents in packaging for food storage—although this is not viable for biological preservation. Similar works into frost formation with the observation in temperature fluctuations were conducted by Urquiola et al. [18]. The study suggests that the current preservation of vegetables using air leads to a deteriorating product quality at both microscopic and macroscopic scales. The research employs CFD simulations to predict airflow for vegetable storage with variations in heat transfer and frost formation. The simulation is based on a 2D schematic due to the geometry of the sliced carrots, with observation of the change in surface temperature. The study itself verifies the accuracy of CFD modelling to determine effective freezing patterns. The use of simulation work is evident when predicting freezing patterns. The most common turbulence models have been simulated for freezing applications. Hu and Sun [19] compared three variations of the k -epsilon model in an industrial food application to observe the most accurate model. The simulation was conducted on an air blast chiller operating at a set point temperature and set airflow speed. The study also observed any weight and moisture loss experienced during the air blast freezing process. The study reflects the under-prediction of the heat transfer coefficient with LRN turbulence models but robust results with both the RNG and standard k -epsilon models accurately predicting the localised heat transfer coefficient.

The process of freezing itself is a vast topic with many available operations such as blast freezing [20], spray freezing [21], immersion freezing [22], and plate freezing [23] being the most commonly used both in cryogenic and mechanical freezing, with each method using a wide range of preservation fluids such as refrigerants, air, carbon dioxide, gaseous and liquid forms of nitrogen. Gaseous and liquid forms of nitrogen are the most common cryogenic fluids used in preservation systems. Although batch freezing is commonly achieved with cooling and the principles of forced convection with the installation of a fan, a large amount of variance occurs. The variance in heat transfer coefficient is due to irregular sample shapes and inefficient storage methods, the most common storage methods being air blast freezers with immersion freezing. To aid blast freezing, a blanching stage may be present before the blast freezing stage. Xin et al. [24] investigated the use of blanching pre-treatments on fresh fruits before high pressure freezing techniques, although the majority of crystals forming on the product was significantly reduced [25,26] with an even product temperature. The techniques for blanching used in multiple studies with a combination of freezing systems, but the scale up of such a technology remains the main issue, alongside operational costs [20,27]. To maximise the economic implementation of cryogenic systems the waste heat recovery of cold temperature exhausts by using thermo-electric modules [28,29]. The same technology has been implemented in LNG vaporisers [30]. The capture of latent heat has been investigated with phase change materials to monitor the change in microcapsules but the scalability of the technology for large biological substances seems unlikely due to the sensitivity of cells with nanoparticles and the associated safety risks [31]. Similarly, the economic use of cryogenics has been implemented within cascade refrigeration systems allowing for an effective refrigerant loop allowing the nitrogen to be separated from liquefied natural gas without the traditional intensive energy processes. The increase possibility of extracted nitrogen can be further implemented in liquidation units for other cryogenic applications. The possibility of localised generation units has been investigated by Ahmad et al. [32] for the implementation of a cryogenic heat exchanger to provide cooling, but the feasibility and application of large-scale

remote within the food preservation industry is yet to be explored due to the masses of space needed for storage tanks for liquid nitrogen, air and the heat exchanger itself.

Rodezno et al. [33] investigated the heat transfer coefficient of catfish fillets with a blast freezing technique using two cryogenic fluids—liquid Carbon Dioxide and air. The results highlighted the increased heat transfer rate and energy rate of a cryogenic system, in comparison to an air-cooled system. The results also highlighted the direct relation between freezing time and the deterioration of quality with a prolonged freezing time. The results reflect that air-cooled systems have a higher moisture content rate in produce compared to a cryogenically cooled system, with the quality further deteriorating in the product storage life span. The process of gas-based blast system is used in large scale systems for the storage of meat carcasses. Hu and Sun [34] conducted a CFD simulation of an air blast freezing method on a large piece of ham. The simulation was based on the air cooling method, but highlights the air and temperature distributions around the freezer. The simulation determined the mass transfer with the consideration of evaporation and condensation of water crystals. Although the simulation is only based on the heat transfer between meat and air, visualisation allows the identification of low heat transfer zones, which can further identify areas of crystallisation and increased moisture content. Similar results are shown by Issa and Lawrence [35] during the experimental heat transfer study of beef carcasses by mist sprays. The experiment involved spraying a cooled air and water suspension onto the carcass. Similarly to Rodezno et al. [33], the moisture content was observed. The freezing time was shown to be considerably larger, with an overall freezing time of 20.9 h. Due to the large scale and complex geometry of the produce, the process of achieving a uniform heat transfer is increasingly difficult [36]. Goral et al. [37] investigated the heat transfer coefficient of vegetables with impingement freezing using air to reach a temperature of -40°C ; similarly as experienced with many air blast systems, the operation of an impingement system is highly dependent on the nozzle type and spray pattern. One of the major observations around an impingement system is the difficulty to maintain a uniform velocity around the product specimen, thus causing variations of the heat transfer coefficient throughout the product. With product temperature being one of the key concerns with cryogenic freezing, a series of heat transfer coefficient collection methods have been employed to monitor localised changes in surface temperature. The collection methods employed by Goral and Kluzza involved a developed flux sensor with a combination of thermo-conductive silicon paste. Amarante and Lanoiselle [38] investigated industrial methods for obtaining the heat transfer coefficient, allowing a localised surface heat transfer coefficient to be calculated. The experimental procedure involved a PVC disc with surface thermocouples installed throughout the thickness of the disc but also two heat flux sensors accounting for conductive and convective thermal effects. Amarante et al. [39] further developed the collection method by implementing flux meters. The principles surrounding the measurement of flux sensors for this particular study involved a series of thermocouples placed within a copper disc set in PVC. Such methods were validated further by Amarante and Lanoiselle [38], with the application of heat flux sensors within industrial freezing equipment to map freezing profiles and processes. The findings of heat transfer coefficient measurement systems reflected areas of insufficient heat transfer alongside the importance of varying refrigerant fluid temperature. Fricke and Becker [40] further developed semi-empirical expressions by developing semi-empirical correlations regarding size and shape of the samples used to aid freezing predictions for numerical simulations.

Meziani [41] investigated the preservation of yeast cultures in

dough, and the resulting fermentation process. The process involved an air freezing method being used in combination with liquid nitrogen immersion freezing. The air blast temperature highlighted a significantly long freezing time of over 4 h, whereas the utilisation of liquid nitrogen managed to freeze the produce in less than 15 min. The results highlighted the maintained gluten integrity with immersion freezing, but significantly reduced the yeast population due to cell damage and the subsequent decreased carbon dioxide production. The preservation of cells has been investigated with singular air blast freezers. The technique proved useful for preventing the potential of cell damage through crystallisation experienced through immersion freezing. Volkert et al. [42] investigated the process of cell preservation—in particular the preservation of bacteria. The experimental study involved spraying air directly onto a petri dish at -30°C . The study presented the potential of using a singular freezing method without damaging cell cultures and fast freezing without immersion freezing. The utilisation of two different freezing methods is evident from the preservation of cell cultures to the preservation of food [22,43]. A similar principle is adopted in the earlier works of cryo-mechanical freezing. Agnelli and Mascheroni [44] adopted a similar principle to freeze a variety of foodstuff. The method used involved the direct contact of liquid nitrogen through immersion freezing. Immersion and conventional freezing methods are commonly used in conjunction with each other due to the fast freezing of one technology and the stability of the other. Earlier works [45] investigated the heat transfer effectiveness of the technology, highlighting the high heat transfer rate of cryogenic freezing, and suggest that the combination of both technologies is the best storage method. However, in comparison with modern freezing methods, the change in technology is minimal. The improvement of the technology is based on the improvement of mechanical parts rather than the freezing method. Individual spray-related systems function on air but with prolonged and inefficient freezing times. The thermal effects of immersion freezing are highly noted in the literature, but the process itself can lead to high levels of crystallisation as a compromise to fast freezing. The application of hybrid blast freezers exist, with air being mixed with liquid nitrogen [46] but a fully cryogenic-based freezer has not been developed. The application of cryogenic fluids for freezing has been used in immersion freezing with fluids ranging from liquid carbon dioxide [47] and liquid nitrogen but a fully cryogenic blast freezing option has not been developed. Gazda [46] investigated the effects of a hybrid system in comparison to an air blast system; the overall exergy of the hybrid model is significantly higher than the conventional method. The findings presented highlight the potential of having one freezing and storage method, and the potential to find an optimum freezing strategy. The findings predict the potential increase in hybrid and fully cryogenic blast methods of freezing. Similarly, the use of injection-based technologies is difficult to predict due to the droplet size, fluid properties, injection type and associated changes in heat transfer. Multiple studies have been conducted on impinging jets in both mechanical and cryogenic freezing applications. Awonorin [48] effectively investigated the heat transfer properties of liquid nitrogen droplets for freezing gelatine bricks but due to the complexities of industrial models and external influences, further predictions about freezing patterns have not been produced. The selection of freezing techniques is dependent on a multitude of factors such as desired freezing time, geometry and the produce, size and economic limitations. Table 1 summarises the applicability of different freezing technologies.

In the present work, the proposed preservation method utilises the thermal potential of liquid nitrogen with the technology behind air blast freezing, allowing for a hybrid system. The preservation will be of glycerine-filled blood bags, with a proposed storage

method investigating the effect of stacking. The freezing process of biochemical substances has not been widely simulated due to the level of complexities existing within the mixture, and the lack of thermal properties available. In this work, the associated change in product core temperature due to shelf loading conditions, product configuration and thermal profiles will be investigated. The results reflect the applicability and effectiveness of such preservation technologies. The investigation is based on two conditions: the determination of the heat transfer coefficient and the performance of the system. Both sets of data will reflect the cooling rate of the chamber but also the effectiveness of processing biological cultures in a continuous operation.

2. Experimental apparatus

There are many experimental freezing methods currently available, ranging from blast freezers to immersion freezing, all utilising different heat transfer mechanisms to effectively freeze and provide effective storage for produce. The freezer used for the experimental observation is a lab scale batch freezer. The operation of the freezer is based on the premise of direct injection of liquid nitrogen into the fan, which distributes cold nitrogen gas around the freezer chamber. The distribution of cold air is conducted using an axial fan, which will distribute cold air to all three shelves and the products placed. The dimensions of the stainless-steel chamber are: $65 \times 50 \times 50$ cm with a volume of 0.16 m^3 . Fig. 1a shows the schematic of the system as an electronic drawing. A schematic of the freezer is shown in Fig. 1b, alongside the loading conditions and placement of the blood bags. The heat transfer coefficient will be conducted on each shelving level and in left right and centre positions as defined in section 3.4.

The operation of the lab scale freezer is based on the principles of forced convection; the activation of the fan will manually distribute the cold gas around the freezer at relatively high velocities to induce freezing. The increase of fan frequency will increase the effects of forced convection resulting in a more uniform heat transfer in a short operating time. Factors such as stacking and positioning also play a key role in the heat transfer mechanism, as previously noted in the literature [36,37]. The stacking location for the batch freezer needs to be loaded in a specific way, the gap between the air and product needs to be 50% of the product depth to allow effective air circulation. A recommended value of 70 mm between blood bags is advised during stack loading.

3. Experimental procedure

3.1. Temperature monitoring

To characterise the thermal performance of the system, 10 T-type thermocouples were placed inside the blood bags to monitor the changes of the core temperature. 1 Thermocouple were also placed within the freezer monitoring changes in air temperature. The lab scale freezer itself also contains a probe providing live monitoring.

3.2. Velocity reading

Due to the thermal restrictions of anemometers, a series of velocity readings were conducted using a pre-calibrated conventional handheld anemometer (Testo 425). The velocity readings were mapped at -10°C at a steady point temperature via an integrated automatic control system. The readings were conducted at fan speeds of 285RPM and 1995RPM. The positions of velocity readings are shown in Fig. 2a and b.

Table 1
Comparative table of freezing techniques.

Preservation Method	Process Load	System Operation	System Drawbacks	System Advantages
Immersion Freezing [22,47,49,50]	Batch	Products are placed within a porous bag and immersed within a fluid. The fluid is a compatible refrigerant or freezing fluid.	<ul style="list-style-type: none"> • Potential for cross contamination • Large system footprint • Limited amount of bio-compatible immersion fluids • Dated preservation technology • Potential for crystallisation and cellular level damage 	<ul style="list-style-type: none"> • Allows for continuous freezing processes • Quick freezing time • Minimal down time
Plate freezing [23,38,51–54]	Batch	Products are arranged in-between two freezing plates; the plates contain a cooling coil. When in contact with product, the coil cools the plate via conduction.	<ul style="list-style-type: none"> • Inconsistent temperature • Inconsistent freezing patterns which is dependent on the placement of sensors • Significant amount of maintenance time required • Unsuitable for continuous operation 	<ul style="list-style-type: none"> • Cost effective systems • Small footprint • Maximises available volume of the system • Vast amount of compatible and available refrigerants • Minimal risk of cross contamination
Injection Freezing [21,55–59]	Continuous	Product is loaded into a system where a jet of cryogenic fluid is sprayed. Typically, this is on a continuous bed to achieve mass amounts of freezing in a short amount of time	<ul style="list-style-type: none"> • High rate of refrigerant consumption • Direct contact with cryogenic fluid creates high levels of crystallisation 	<ul style="list-style-type: none"> • Suitable for continuous freezing and operation. • Allows for mass production
Individual Quick Freezing [24,60–63]	Singular	Single product is placed within chamber space where a cryogenic fluid is sprayed directly onto the product.	<ul style="list-style-type: none"> • Ineffective for mass production due to large processing time • Irreversible damage to cells due to multiple cell types within one system • Efficient thawing process currently unavailable • Uneconomical for small products • Cannot be used for food processing due to the high level of cellular damage 	<ul style="list-style-type: none"> • Suitable for large complex products such as carcasses and livestock • Quick freezing and processing time • Can be applied for medical applications where aesthetic is not the main concern
Conventional Slow Freezing [31,61,64–66]	Batch	Commonly used in hybrid systems where items are quickly frozen and then placed within slow freezing using conventional freezers.	<ul style="list-style-type: none"> • Prolonged freezing time • Cannot be used for mass freezing production • Commonly used within hybrid systems for storage. 	<ul style="list-style-type: none"> • Ideal of storage solutions • Components readily available • Suitable for continuous use • Cost Effective
Isochoric Freezing [67–71]	Batch	Products are lowered into a pressurised vessel containing solution that is of equal osmotic concentration than the sample. The product is brought to a thermal equilibrium between water and ice formation within the cells.	<ul style="list-style-type: none"> • Unsuitable for long term storage • Relatively new technology, potential for scale up poses to be a problem • Unknown processing functions, capabilities for continuous processing is currently unknown. 	<ul style="list-style-type: none"> • Preserves cell quality by preventing osmotic changes occurring during conventional freezing techniques. • Emerging freezing technology



Fig. 1. a: 3D Render of Batch Freezer (b) Lab scale set up of Batch Freezer.

3.3. Blood bag positioning

The positioning of blood bags is shown in Fig. 2b. They are placed in single and double stack configurations. To ensure uniformity across all the blood bags, the specimens are conventional blood transfusion bags with identical dimensions and a 600 ml limit. The blood bags have been filled with water and glycerine, with a ratio of 9:1 respectively.

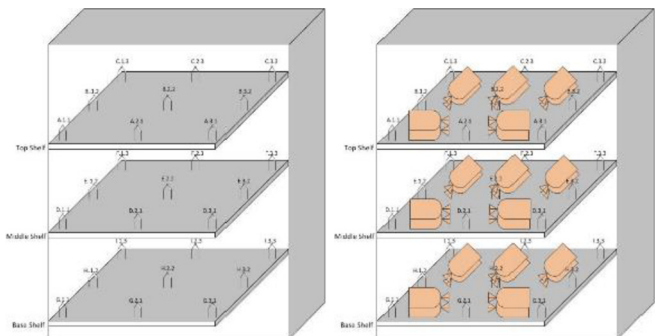


Fig. 2. a Velocity measurement schematic (empty) (b) Velocity measurement schematic (fully loaded).

3.4. Heat transfer coefficient observation

The heat transfer coefficient was measured with a heated copper disc and monitoring the cooling rate of the freezer system as

shown in Fig. 3. The heat transfer coefficient study acted as a baseline and was conducted with an unloaded configuration. The heat transfer coefficient can be calculated by:

$$h = \frac{m \cdot C_p \cdot \left(\frac{DT}{\Delta t}\right)}{A \cdot \Delta T} \quad (1)$$

where:

- h is the mean heat transfer coefficient (W/(m².°C))
- A is the surface area of the copper disc (m²)
- ΔT is the temperature difference between the mean product temperature during the freezing process and the freezer's air temperature (°C)
- m: mass (kg)
- C_p: Specific heat (J/(kg.°C))
- DT: Difference in disc temperature (°C)
- Δt : Difference in time (s)

The procedure involves the heating of copper discs, containing a thermocouple to monitor and record their cooling rate. The discs are placed within a pre-defined temperature water bath to heat them up to 80 °C. The temperature of the discs is kept constant. The placement and use of the copper discs are dependent on the set point temperature of the freezing system. The system will aim to reach the set point temperature and allowing for a period of steady state operation. The heated copper burgers are placed within the system and allowed to cool to observe the cooling rate of the system. The obtained data allows us to estimate an average heat transfer coefficient.

4. CFD model

Computational Fluid Dynamics (CFD) is an increasingly utilised technology which determines a fluid flow field by solving the governing flow equations, i.e. momentum, continuity and energy equations as highlighted below:

Conservation of Mass:

$$\frac{\partial U_j}{\partial x_i} = 0 \quad (2)$$

The conservation of mass (continuity) equation highlights the balance in masses between the inlet and outlet.

Conservation of Momentum:

$$\rho \frac{\partial U_j}{\partial t} + \rho U_i \frac{\partial U_j}{\partial x_i} = -\frac{\partial P}{\partial x_j} - \mu \frac{\partial^2 U_j}{\partial x_i^2} + \rho g_j \quad (3)$$

The momentum equations utilised during the simulation reflect the laws of motion represented as stress tensors. The equations highlight the change in momentum with local changes in time and surface tension. The first part of the equation highlights the change in time and convection, with the latter part representing diffusion and surface/tensile forces.

Conservation of Energy:

$$\rho c_\mu \frac{\partial T}{\partial t} + \rho c_\mu U_i \frac{\partial T}{\partial x_i} = -P \frac{\partial U_i}{\partial x_i} + \lambda \frac{\partial^2 T}{\partial x_i^2} - \tau_{ij} \frac{\partial U_j}{\partial x_i} \quad (4)$$

The energy equation accounts for changes in the internal energy within the system. The first half of the equation represents the change in time and the influence of the convective term. The latter half represents pressure, heat flux through diffusion and irreversible heat transfer. The equation is based on the first law of thermodynamics.

The tool uses the problem geometry with an applied set of boundary conditions to characterise the flow field in the system. The tool requires a significant amount of computational power depending on the application. CFD is a powerful tool able to model complex processes ranging from multiphase models, combustion models and even chemical reactions alongside the modelling of the interaction between solids and liquids [72]. The development of CFD has led to an increased accuracy in predicting system performance and reliability of computational models. The prediction of temperature distribution has been investigated in many preservation applications, with the majority investigating effective storage methods. The results obtained from CFD simulations highlight the fluctuations in heat transfer alongside the identification of poor heat transfer zones. The CFD model used to simulate the freezer is based on the rotating fan geometry enclosed within a box with the exact dimension and volume of the freezer. The positioning of the blood bags is as shown in the proposed shelf configurations. The proposed CFD geometry was constructed in ANSYS DesignModeller as a three-dimensional computational model. To mimic the thermal profile of the freezer, a user-defined function (UDF) was compiled to simulate the change in air temperature as the liquid nitrogen spray is activated, alongside a transient solving algorithm.

4.1. CFD methodology

ANSYS Fluent was the chosen Computational Fluid Dynamics (CFD) software to simulate the heat transfer mechanism within the freezer. The proposed model will effectively represent the heat transfer with the influence of a swirling flow induced by an axial fan. The k-epsilon turbulence model was activated alongside the effects of scalable wall functions to increase the stability of the system. The process for the heat transfer itself is based in the governing energy transport equation. As the simulation is based on the disengagement of liquid nitrogen injectors, the operating gas within the chamber is assumed to be a single-phase nitrogen gas. The chosen wall boundary conditions model accounts for coarser meshes located near walls, and the consideration of a swirl dominated flow [73]. The fan was simulated using a moving reference frame method with the definition of pressure-velocity coupling for increased simulation stability.

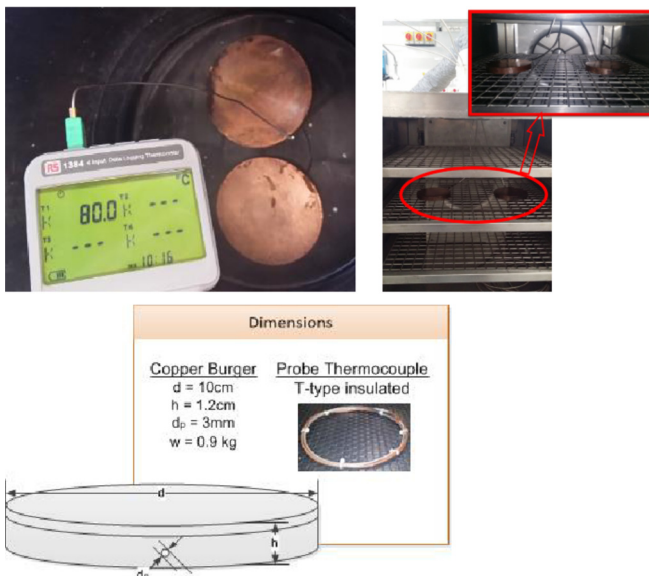


Fig. 3. Experimental set up and methodology of the heat transfer coefficient.

Table 2
Mesh sensitivity study.

Level	Number of Cells	Cell Type	Skewness	Time per Iteration
Coarse	506,402	Hexahedral	0.656	5–10s
Coarse	566,030	Tetrahedral	0.701	5–10s
Medium	1,402,790	Hexahedral	0.732	10–12s
Medium	1,497,204	Tetrahedral	0.759	10–14s
Fine	2,059,241	Hexahedral	0.895	15s+
Fine	2,504,259	Tetrahedral	0.851	15s+

4.2. Assumptions

The following assumptions were made prior to conducting the simulation:

1. The thermal profile of the injector has been utilised rather than a physical model of the injector to mimic the cooling profile of the system.
2. The glycerine bags are all initially set at a uniform temperature of 17 °C.
3. No heat transfer occurs at the walls of the freezer; thus, the relevant zones have been set as adiabatic regions.
4. The presence of liquid nitrogen will not be included—only the gaseous phase.

4.3. Mesh refinement study

A mesh refinement study was initially conducted to verify the accuracy and efficiency of the mesh. The different meshes were selected by analysing the skewness of each mesh density and cell type. Typically, a mesh of skewness under 0.7 is considered to be a good mesh for a hexahedron mesh type and 0.8 for a tetrahedral mesh. The results obtained from the mesh refinement study are shown in Table 2.

The results obtained from the mesh refinement study highlight the increased performance with a structured hexahedral mesh compared to an unstructured tetrahedral mesh. The uniformity of the mesh ensures the correct density near walls when simulating a swirling flow. The overall results obtained from the mesh independence study highlight a skewness of 0.895 for the fine

hexahedral mesh, and 0.851 for the fine tetrahedral mesh. The simulation time for all mesh densities shows an increase in simulation time as the mesh density increases, with a reflected increase in accuracy. The mesh density between medium and fine reflects an increase in accuracy of approximately 13%; therefore, a fine mesh was applied throughout the simulation. The mesh sensitivity study was conducted with the default relaxation factors, with a residual tolerance set at 1e-8.

4.4. Boundary conditions

To define the inlet and outlet profiles, a pressure velocity coupling was applied throughout the entire schematic. As the fan rotation is the dominant feature, a *Velocity Inlet* of 0.001 m/s was applied in the fan flow direction as initialisation. The boundary conditions selected also account for the thermal changes within the freezer with the operation of the injectors as experienced in the lab scale system. The UDF profile is based on an experimental profile, obtained with each test as a function of time to reach a set temperature. The outlet was set as a *Pressure Outlet* at the exhaust.

4.5. User defined function (UDF)

The development of a user defined function is primarily compiled in C++ and applied to the fluid properties within the glycerine filled bags. The UDF starts at an arbitrary loading temperature of 20 °C, with the only variable being the set point temperature. To accurately simulate the phase change phenomena occurring in the process, a UDF was created based on the energy required to reach the phase change point, based on the thermo-physical properties of glycerine and water. The duration of phase change is independently based on the freezing profile of the glycerine and water mixture, with the duration to the set point being based on the energy required to reach the set point.

5. Results and discussion

5.1. Experimental results

5.1.1. Air flow velocities

Air velocity measurements were taken in an empty and a fully loaded freezer at 285 RPM and 1995 RPM. The relative positions for

Table 3
Empty freezer velocity measurements.

	Empty Freezer			
	285 RPM		1995 RPM	
	Loading Location	Velocity Reading	Loading Location	Velocity Reading
Top Shelf	C1.3	1.06 m/s	C1.3	7.24 m/s
	C2.3	0.68 m/s	C2.3	2.12 m/s
	C3.3	0.69 m/s	C3.3	2.10 m/s
	A1.1	0.62 m/s	A1.1	3.03 m/s
	A2.1 (No Load)	0.72 m/s	A2.1 (No Load)	3.82 m/s
	A3.1	0.54 m/s	A3.1	3.79 m/s
Middle Shelf	F1.3	1.16 m/s	F1.3	4.12 m/s
	F2.3	1.31 m/s	F2.3	8.75 m/s
	F3.3	0.67 m/s	F3.3	3.86 m/s
	D1.1	0.50 m/s	D1.1	3.3 m/s
	D2.1 (No Load)	0.70 m/s	D2.1 (No Load)	3.92 m/s
	D3.1	0.39 m/s	D3.1	2.73 m/s
Bottom Shelf	I1.3	0.59 m/s	I1.3	4.54 m/s
	I2.3	1.41 m/s	I2.3	8.43 m/s
	I3.3	0.47 m/s	I3.3	5.46 m/s
	G1.1	0.42 m/s	G1.1	2.59 m/s
	G2.1 (No Load)	0.91 m/s	G2.1 (No Load)	4.88 m/s
	G3.3	0.49 m/s	G3.3	2.59 m/s

Table 4
Fully loaded freezer velocity measurements.

	Full Freezer			
	285 RPM		1995 RPM	
	Location	Velocity Reading	Location	Velocity Reading
Top Shelf	C1.3	1.77 m/s	C1.3	3.52 m/s
	C2.3	0.54 m/s	C2.3	3.66 m/s
	C3.3	0.71 m/s	C3.3	2.51 m/s
	A1.1	0.68 m/s	A1.1	3.64 m/s
	A2.1 (No Load)	0.44 m/s	A2.1 (No Load)	1.99 m/s
Middle Shelf	A3.1	0.94 m/s	A3.1	2.75 m/s
	F1.3	0.88 m/s	F1.3	5.72 m/s
	F2.3	1.53 m/s	F2.3	10.3 m/s
	F3.3	1.02 m/s	F3.3 <td 4.84 m/s	
	D1.1	0.51 m/s	D1.1	3.16 m/s
Bottom Shelf	D2.1 (No Load)	0.52 m/s	D2.1 (No Load)	2.61 m/s
	D3.1	0.73 m/s	D3.1	2.07 m/s
	I1.3	0.76 m/s	I1.3	4.41 m/s
	I2.3	1.64 m/s	I2.3	9.58 m/s
	I3.3	0.78 m/s	I3.3	3.74 m/s
	G1.1	0.44 m/s	G1.1	1.61 m/s
	G2.1 (No Load)	0.76 m/s	G2.1 (No Load)	4.24 m/s
	G3.3	0.56 m/s	G3.3	2.39 m/s

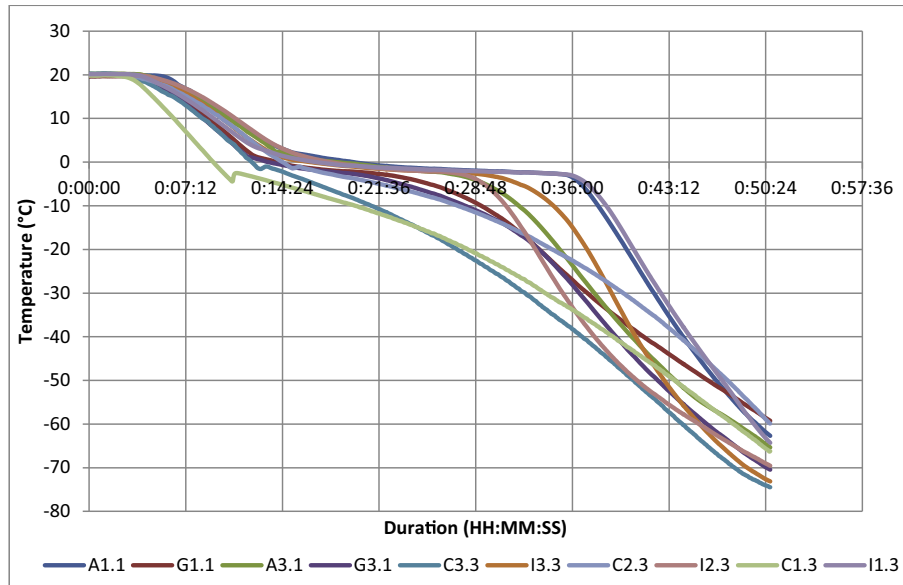


Fig. 4. Freezing profile of glycerine filled blood bags.

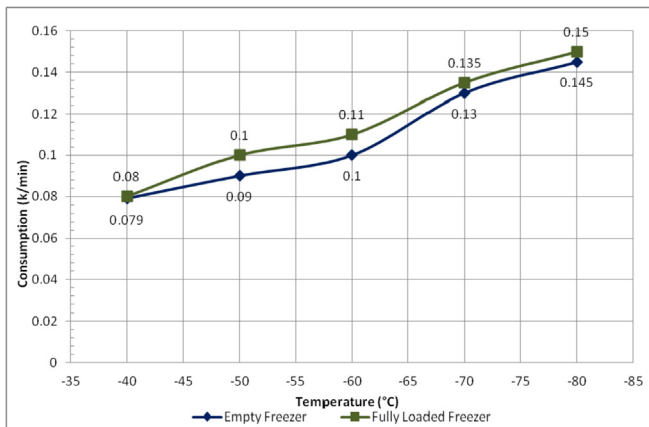


Fig. 5. Liquid nitrogen consumption.

the velocity readings for an empty freezer are shown in Fig. 2a. The readings taken are shown in Table 3.

From the results obtained, the locations of low velocity zones have been identified highlighting potential low performing heat

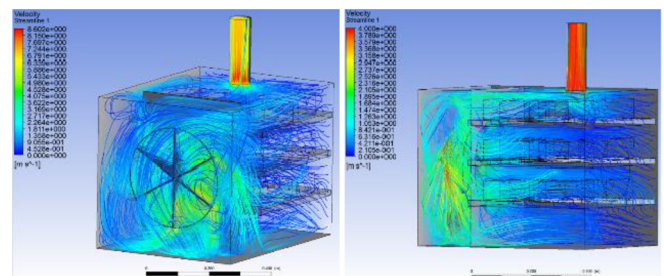


Fig. 6. Streamlines for a double stack system at 1995 RPM

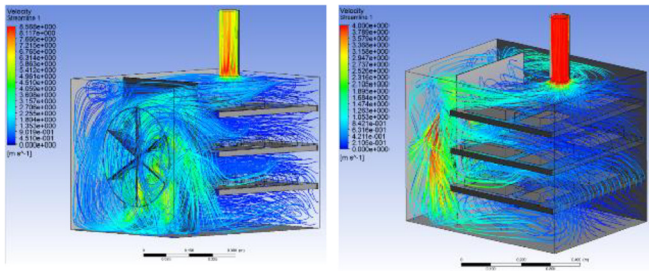


Fig. 7. Streamlines for a single stack system at 1995 RPM

transfer zones. Both fan configurations have high velocity areas in some zones. The high speed and low speed zones are highlighted in the table in red and blue, respectively.

Table 3 and Fig. 2b show the velocity recordings and probe positions of a fully loaded freezer. The readings for both 285 RPM and 1995 RPM are shown in Table 4.

The results in Table 3 show an improved air distribution as the effect of the loading and the corresponding velocity changes as a result of turbulence. The results show an overall increase and a more even distribution of air at a lower RPM value between both

loaded and unloaded freezers. During a higher RPM operation with a full load, the majority of the recorded values are high velocities, giving a preliminary indication of a high heat transfer area.

5.1.2. Default operating conditions

The initial operation of the system was conducted at a high RPM (1995 RPM) for a single stack loading configuration. The glycerine filled blood bags were loaded at an ambient core temperature of 20 °C, and the observed temperature profile was gathered from the ambient starting point up to -70 °C. The results are shown in Fig. 4. The loading locations of the bags are shown in Fig. 2.

The temperature profile (Fig. 4) experienced during the operation highlights an effective and steady freezing profile. Unlike other direct contact freezing methods, sharp temperature decreases are not seen in this process as experienced with immersion freezing. The lack of sharp temperature decreases also indicates the lack of crystallisation, leading to a higher quality produce. The graph suggests that blood bags located in zones C1.3 and C3.3 experience the sharpest decrease with spikes in temperature, due to the positioning of the bags in relation to the injector. Similarly, zones G1.3 and G3.1 reflect areas of high temperature due to a lack of recirculation. The middle spectrum of temperatures reflects a steady temperature decline with minimal temperature spikes.

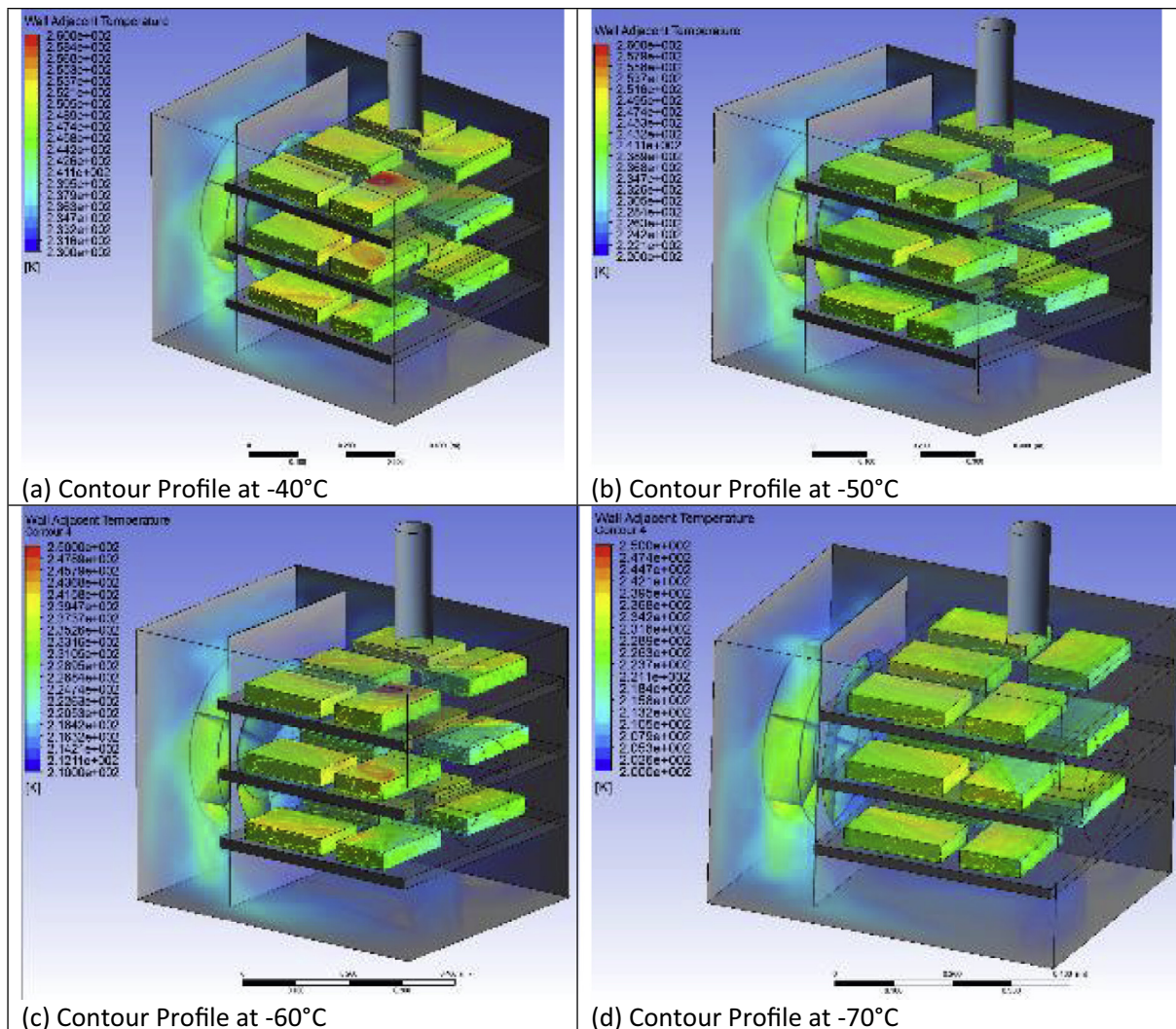


Fig. 8. Temperature contour plot of freezer operation.

5.1.3. Liquid nitrogen consumption

The consumption of liquid nitrogen was monitored throughout the test duration with its weight being recorded at the beginning and at the end of each test. The monitoring of liquid nitrogen consumption was carried out by recording the weight difference between each test for each temperature profile, calculated by using equation (5). The liquid nitrogen consumption for each temperature profile is shown in Fig. 5.

$$w = \rho \cdot v \tag{5}$$

where:

w is the weight difference of the tank before and after the experiments (kg).

ρ is the density of liquid nitrogen, which is 0.808 kg/L.

5.2. CFD results

The observed velocity streamlines demonstrate the operation of a high RPM using a double stack schematic (Fig. 6) and a single stack schematic (Fig. 7). The streamlines highlight the change in resistance in the system, with the reflected change in the maximum velocity. Fig. 6 shows the maximum velocity at 8.6 m/s, with an average velocity of 3.62 m/s throughout the shelf distribution. The velocity streamlines for a double stack system show a relatively high velocity around the bags located close to the fan. There is an increase in velocity through the exhaust system and surrounding

area, highlighting a potential area of increased convection. The streamlines depict an increase in velocity through the sides of the system but a lower velocity closer to the system extremities. The low velocity areas in a single stack (Fig. 7) located away from the fan highlights the potential area of high temperature variation. In comparison to a single stack system the maximum velocity is lower by 0.04 m/s, and similarly the sides of the system show an increase in velocity passing through the sides. The increase in velocity highlights an area of increased convection, thus demonstrating an improved freezing pattern. Unlike the double stack configuration, the single stack configuration depicts an increased velocity due to the lack of resistance towards the outer edge of the system.

5.2.1. Temperature contour profile

The contour plots presented in Fig. 8 represent the variation in temperature during the freezer operation between -40 °C and -70 °C. The temperature contour plot at -40 °C shows a large amount of temperature variation in comparison to the other temperature contours, which may be due to the increased liquid nitrogen injection because of the -70 °C set point. The temperatures observed during operation at -40 °C (Fig. 8a) show a significant variation on the upper surface of the block. The temperature variation on the surface towards the back of the system furthest from the fan shows a significantly lower temperature in comparison to adjacent placed bags. The variation in temperature in these regions highlight strong recirculation zones within those areas, similarly the areas depicted as having higher temperatures are due to the high-speed flow, poor recirculation due to the vacuum effect

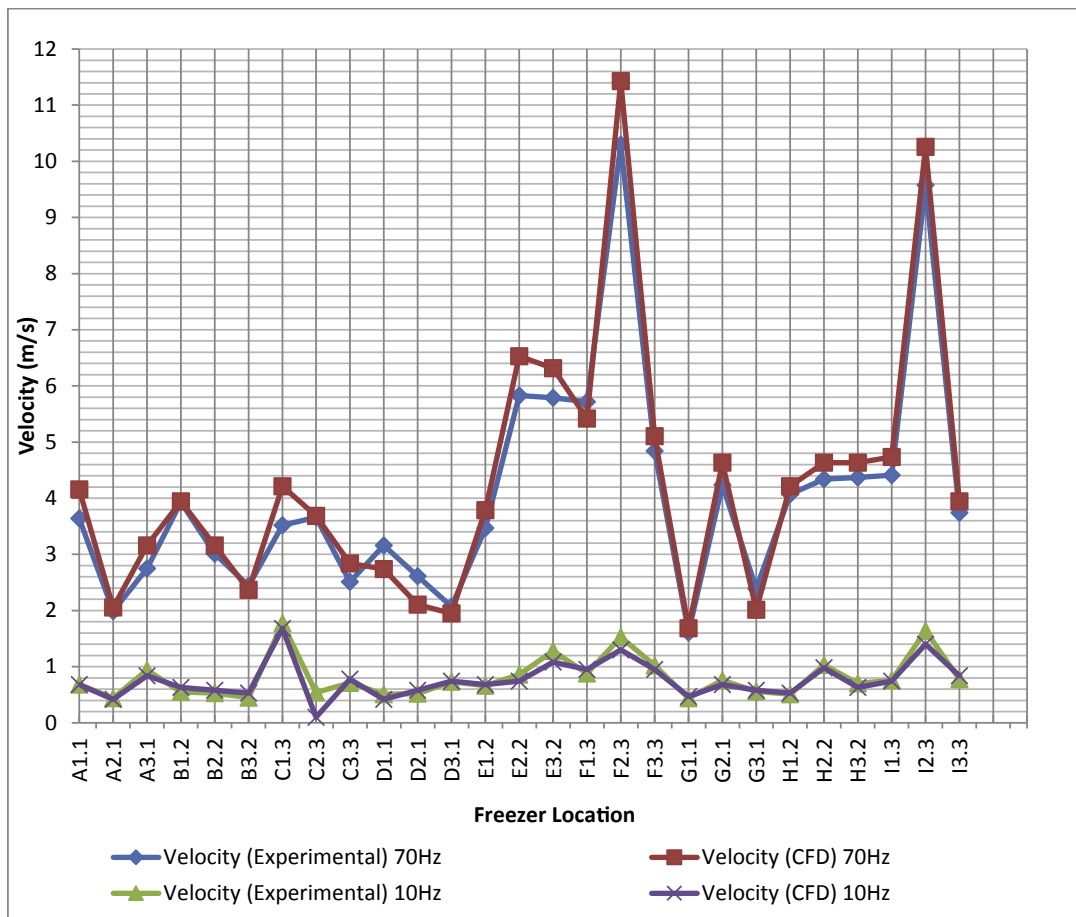


Fig. 9. Velocity profile for both CFD and experimental values.

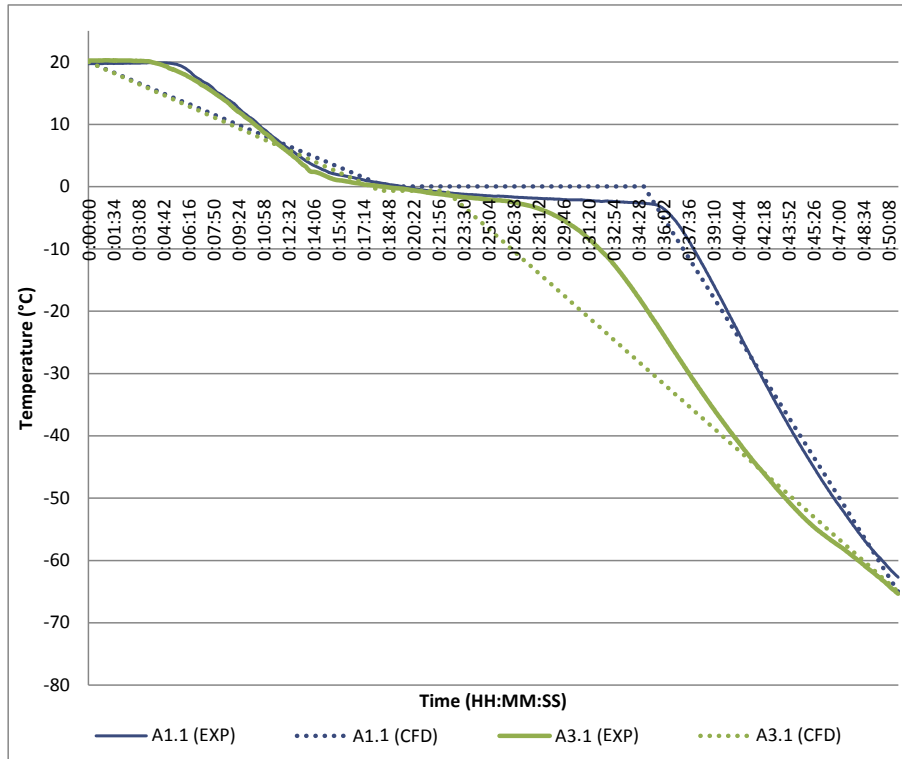


Fig. 10. Experimental and CFD temperature profiles for Zone A.

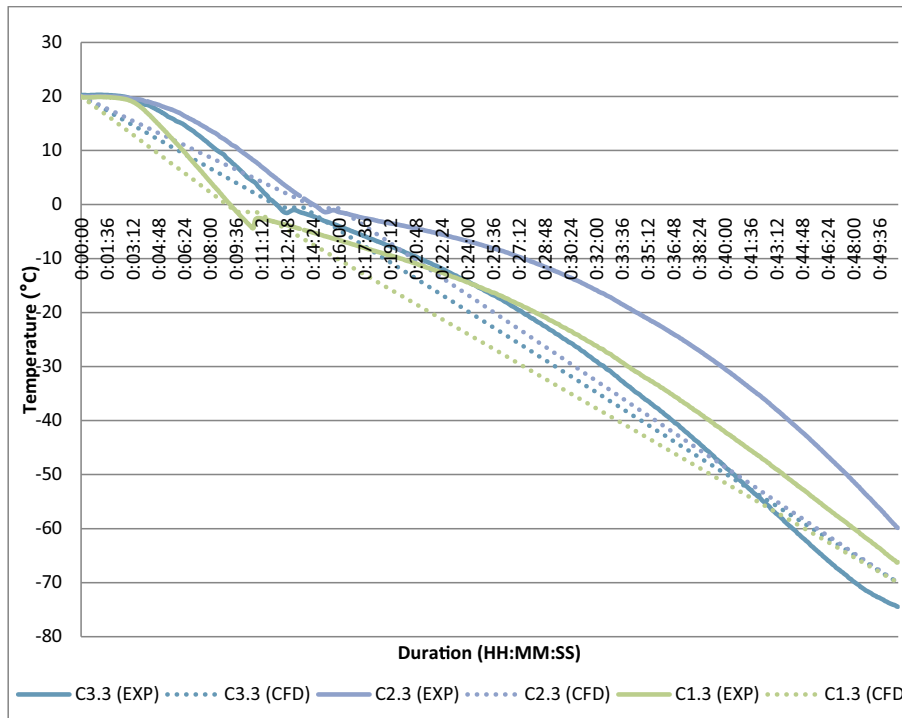


Fig. 11. Experimental and CFD temperature profiles for Zone C.

created by the exhaust and frictional effects within the regions. Fig. 8b shows the contour plot at -50°C ; unlike the -40°C operation, the decrease in temperature variation reflects a significantly increased uniformity due to the increase in liquid nitrogen injectors

lowering the air temperature and associated heat transfer between the product and air. The circulation towards the back of the freezer is reflected in the stability of temperatures with an average bag core temperature deviation of 10 K. Fig. 8c shows the operation

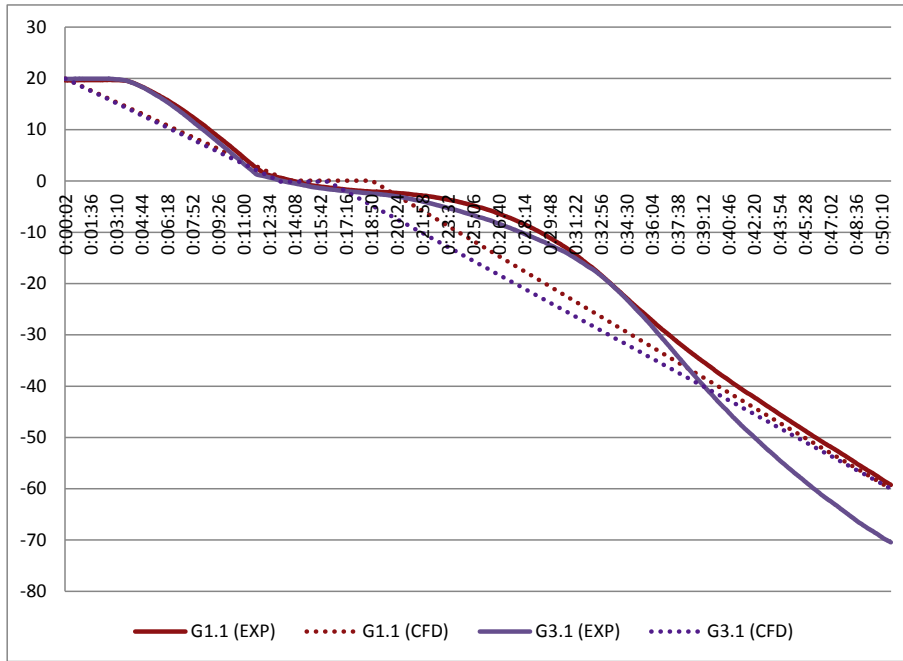


Fig. 12. Experimental and CFD temperature profiles for Zone G.

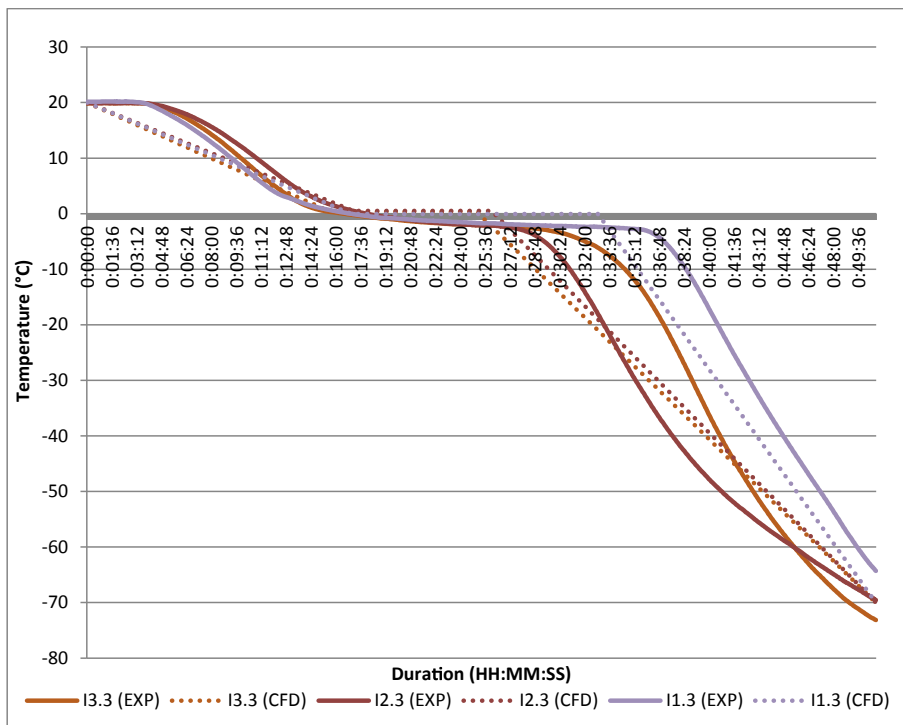


Fig. 13. Experimental and CFD temperature profiles for Zone I.

at $-60\text{ }^{\circ}\text{C}$, with similar results as $-50\text{ }^{\circ}\text{C}$. The results show a slight increase in temperature near the exhaust region highlighting the lack of recirculation in the area, and the change in temperature profile due to suction. Fig. 8d shows the operation at a set point temperature of $-70\text{ }^{\circ}\text{C}$, the temperature difference experienced by the glycerine filled blood bags is minimal with the average system difference being around 5 K.

5.3. Validation

5.3.1. Velocity profile

Both experimental and numerical velocity readings were taken in corresponding positions, for both high and low fan speed configurations and as a double stack. The velocity readings obtained are shown in Fig. 9, according to the positioning schematic shown in Fig. 2a and b. The CFD results depict the expected over-prediction

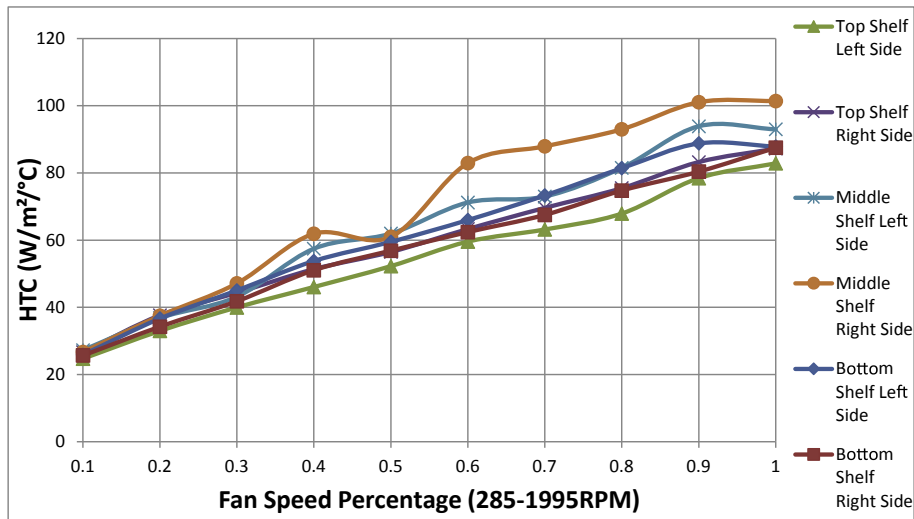


Fig. 14. Heat transfer coefficient at -40°C .

of velocity values, due to many factors such as instrumentation errors and turbulence model over-predictions. Both experimental and CFD values show a similar trend with an average velocity variance of 16%. The corresponding high RPM shows a higher amount of variance; this may be due to many reasons such as the physical movement of the probe due to increased velocity. The corresponding low velocity measurements highlight a less varied velocity result with an average velocity variation of 9% between CFD and experimental results.

5.3.2. Blood bag temperatures

Zone A.

The position of Zone A is shown in Fig. 2b with the corresponding loading configuration highlighted in the figure. Fig. 10 shows the CFD and experimental temperature profiles for Zone A, located towards the extremities of the system towards the exhaust. Both CFD and experimental values show very similar trends, with

the CFD values showing a slight under-prediction of 12.4%, with both following the overall trend of the experimental data. Both experimental and CFD results show a prolonged horizontal period when the core temperature reaches freezing point due to the transfer of latent heat to the surroundings. Zone A is also located near the exhaust and influenced by the vacuum properties created from the exhaust during operation. The thermal effects of the glycerine-filled bags at these locations are discussed in section 5.2.2 with the aid of contour plots. The variation in temperature between zone A1.1 and zone A3.1 is due to the positioning of each bag, despite them being in the same zone. The temperature variation between both bags highlights the effect of the exhaust suction, with zone A1.1 being most affected by the exhaust causing a delayed freezing to reach the desired set point. Both sets of experimental and CFD data show a steady and smooth decline in temperature.

Zone C.

The positioning of loads in zone C is shown in Fig. 2a and b. Zone

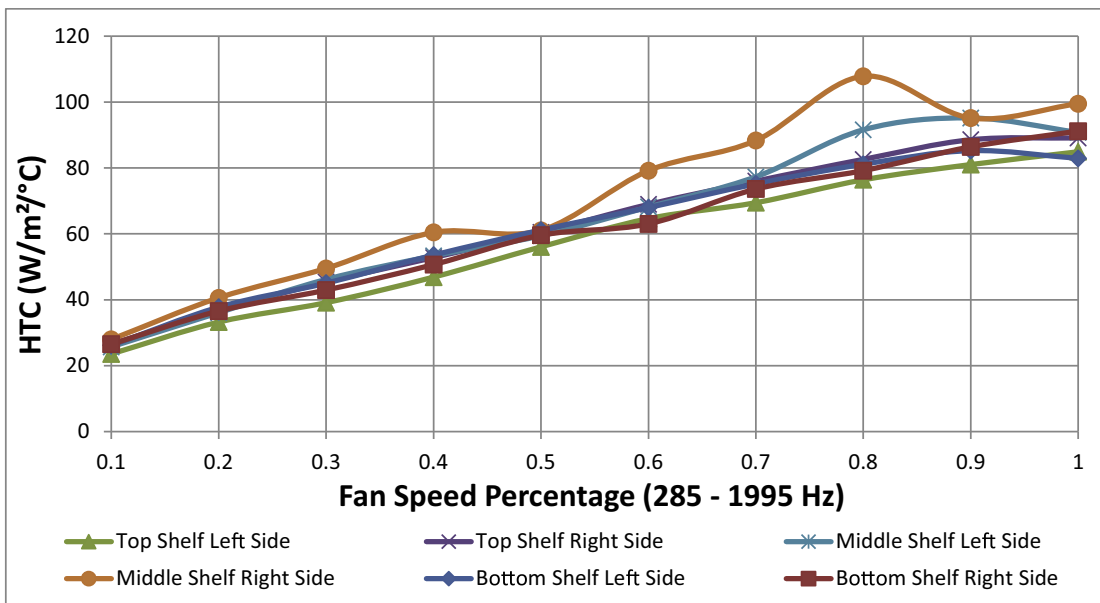


Fig. 15. Heat transfer coefficient at -50°C .

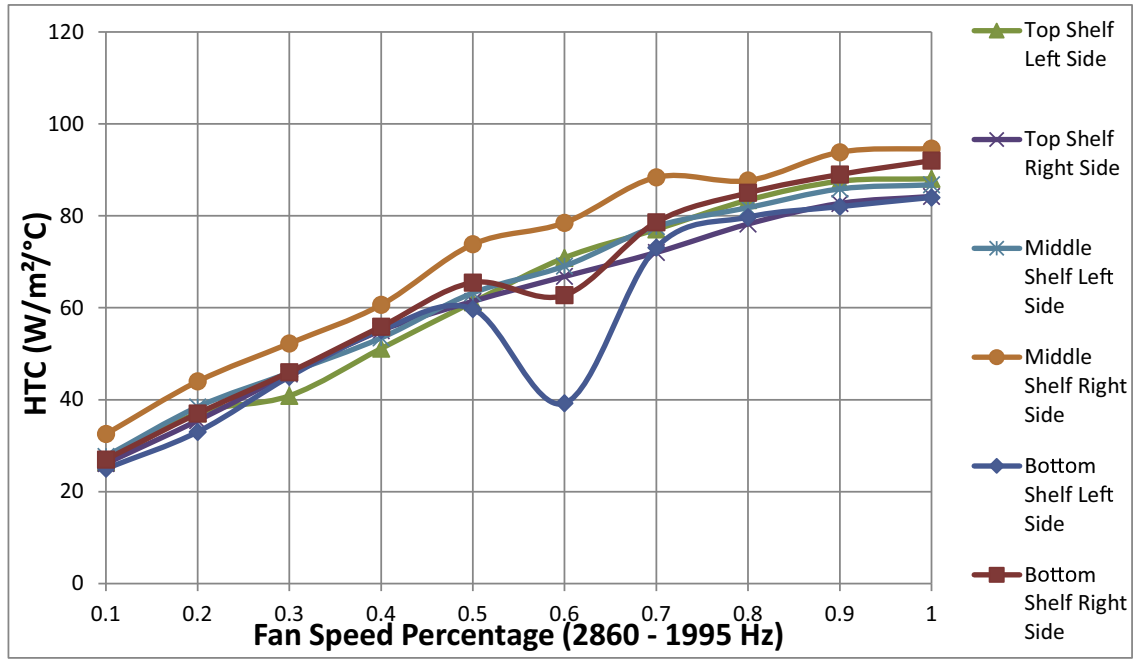


Fig. 16. Heat transfer coefficient at -60°C .

C is located closest to the injectors on the top shelf. The experimental data show a singular sharp spike in temperature due to the increase in injection resulting in droplets interacting with the surface of the bag, as shown in Fig. 11. The CFD data for zones C1.3, C2.3 and C3.3 do not reflect this spike in temperature due to the UDF applied to the load in zone C. The UDF implies a phase change point which is significantly higher than the experimental data. As the UDF is based on an arbitrary profile, a level of variation exists during the phase change stage. The experimental results reflect a sudden but small spike in temperature due to the proximity to the injectors. The results highlight a steady decrease. Similarly to previous results, the UDF does not highlight the horizontal period

experienced experimentally at the start of the test. The lack of horizontal period reflected in the experimental sets of data highlight a quicker transfer of latent heat in the specific area. The temperature variation between experimental and CFD data highlights a smooth decline to the set point temperature. The CFD UDF utilised overpredicts the freezing pattern for zones C2.3 and C3.3. The average variation between the loading conditions to reach the set point temperature has a maximum difference of 52.5% and 45.5%, respectively, in comparison to 27.2% in zone C1.3. The over prediction is more pronounced in the results for the phase change point to the set point.

Zone G.

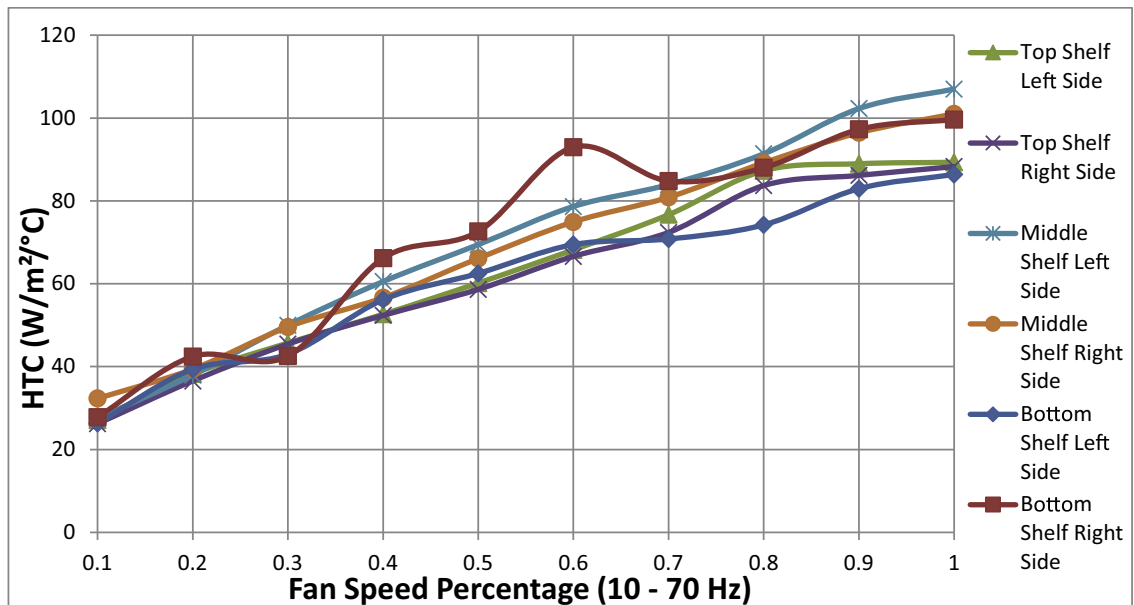


Fig. 17. Heat transfer coefficient at -70°C .

The location of zone G is also shown in Fig. 2a and b, indicating the position of the glycerine-filled blood bags. The relative location of Zone G is on the bottom shelf, located close to the freezer door. The temperature profile of the bags is shown in Fig. 12 for both experimental and CFD data. The loading position in comparison to zone A follows a similar trend due to the translational proximity between both zones. The data reflects the progressive decrease to the set point temperature without sudden temperature spikes. The UDF applied to zone G highlights a prominent over prediction in zones G1.1 and G3.1. The maximum overprediction between the experimental and CFD results for zone G1.1 differs by 55% in comparison to G3.3 with an overprediction of 69%. Both zones reflect a steady decline to the set point temperature. The location of zone G itself is towards the back of the system and indirectly placed from the exhaust system. The steady decline is reflected in the location as the thermal variations experienced with suction are significantly reduced for both sets of data. The lack of suction also allows recirculation of the area and the bottom shelf. This is evident due to the relatively shorter horizontal period reflecting an increased transfer in latent heat between the gas and glycerine filled bags. As

experienced with all numerical simulations, a level of difference will always exist between numerical prediction and the obtained experimental results.

Zone I.

Similarly to zone G, zone I is located directly beneath zone C and follows an identical loading pattern as shown in Fig. 2a and b. Fig. 13 depicts both CFD and experimental sets of data. Zone I is located just under the injector profile. Both CFD predictions for zones I2.3 and I3.3 highlight a relatively significant over prediction with a maximum difference of 46.5% and 96.1% between CFD and experimental results. Unlike previous data sets, a small amount of under prediction exists in Zone I2.3 between -22°C and -70°C , which may be due to the assumption of a steady decline to the set point temperature. Unlike zone C, the temperature profile of zone I shows a horizontal profile in which transfer of latent heat is occurring. As the glycerine-filled bags are located furthest away from the exhaust, the relatively prolonged freezing time may be due to the poor recirculation within the region. The trend is discussed in section 5.2.2, showing an increased temperature along the upper surface of the bags highlighting a region of poor

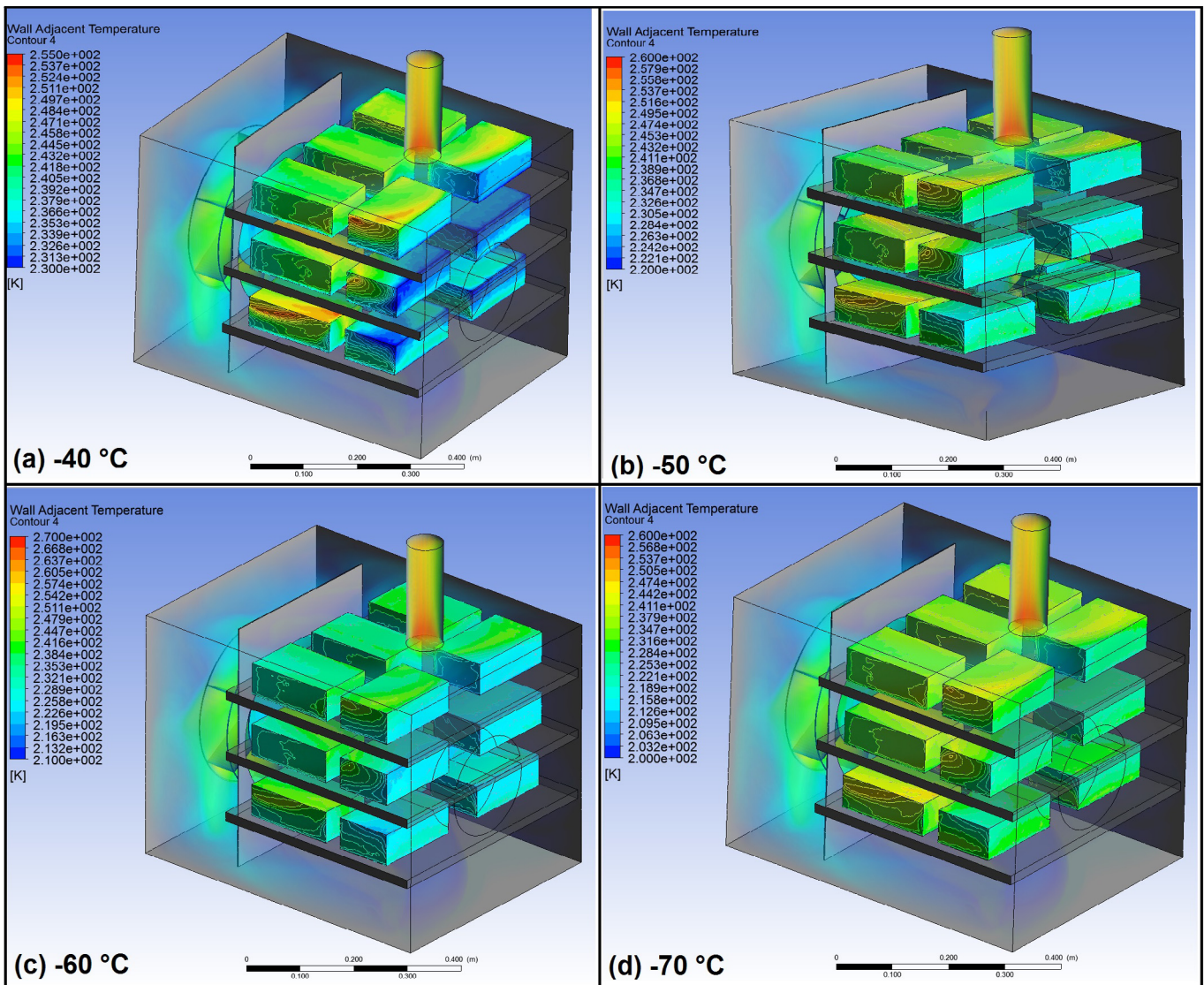


Fig. 18. Temperature contour plot of double stack loading at 285 RPM

recirculation. The region of poor recirculation is evident because of the temperature variation between each zone shown in section 5.2.2. The recirculation primarily affects the transfer of latent heat but, after the freezing point has been reached, the zone experiences a rapid decrease in temperature to the set point.

5.4. Heat transfer coefficient

The reflected experimental results shown in Figs. 14–17 highlight the associated heat transfer results. The heat transfer coefficient study was conducted as a baseline experiment to gather initial observations about the system. The observation of the system was conducted with the copper specimen as mentioned in section 3.4.

5.4.1. -40 °C

The operation at -40 °C reflects the obtained and average heat transfer coefficient of the system as shown in Fig. 14. The heat transfer coefficient obtained reflects a positive trend with an increase in heat transfer coefficient with the increase in forced convection due to the increased fan operation. The data reflects minor

fluctuations due to the change in positioning for each HTC calculation. The level of fluctuation is prevalent in both middle sections on both left and right; this may be due to positioning. The heat transfer coefficient data obtained also reflect potential areas of poor heat transfer.

5.4.2. -50 °C

Unlike the operation in -40 °C, the calculation of the heat transfer coefficient at -50 °C reflects an improved average heat transfer operation due to the larger temperature differential. Both middle shelf locations reflect a higher heat transfer coefficient due to the location of the disc with respect to the flow and impingement direction. The comparison between the -40 °C and -50 °C operations reflect a consistent poor heat transfer zone towards the bottom shelf, as validated through CFD investigations. The data obtained is reflected in Fig. 15.

5.4.3. -60 °C

As expected, the decrease operational temperature increased the temperature differential, therefore resulting in a fractionally

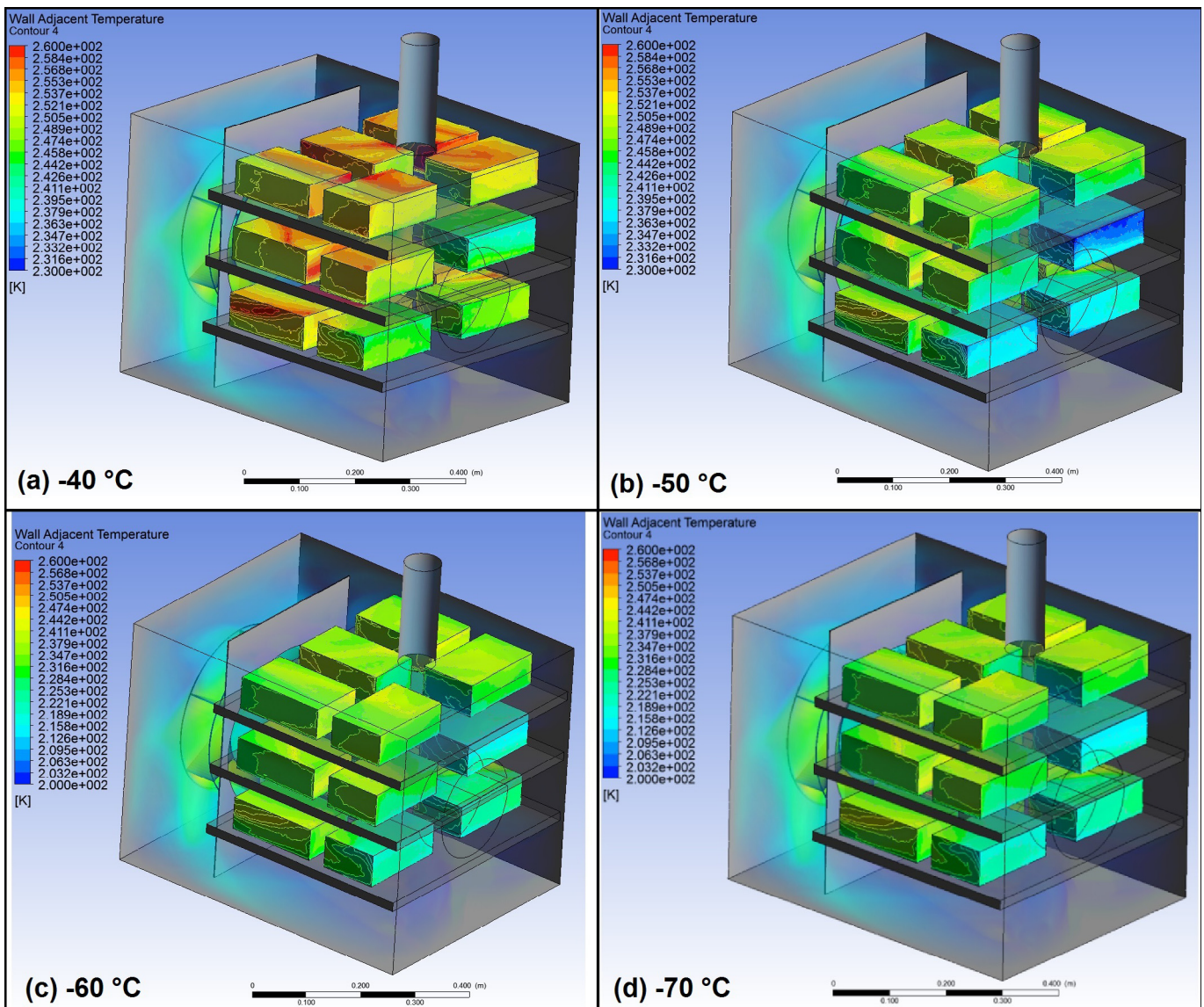


Fig. 19. Temperature contour plot of double stack at 1995 RPM

improved cooling rate as shown in Fig. 16.

5.4.4. -70°C

The final set point at -70°C is reflected in Fig. 17. The data in this figure reflects a substantially large increase in heat transfer coefficient for a 1995RPM operation in comparison to all previous temperature set points. The final set point temperature offers a higher temperature differential and reflected cooling rate. The bottom shelf zones are still predominantly reflecting poor areas of heat transfer as discussed in section 5.2.

6. Proposed additional loading

By utilising CFD, additional loading techniques can be investigated to identify the ideal loading condition and observe the resulting change in the flow profile and associated changes in temperature. The simulations were re-conducted using identical boundary conditions, numerical models and pre-imposed model assumptions, with the only variable being the stacking and change

in RPM. The simulation was re-conducted using a double stack at a high and low RPM, and a single stack at a low RPM.

6.1. Double stack at 285 RPM

The effect of stacking was investigated by placing an additional layer of glycerine-filled bags on top of the existing configuration. The simulation was based on an operation at 285 RPM. Fig. 18 shows the results of the operation of a double stack system at 285 RPM, with a temperature range of -40°C to -70°C . Fig. 18a depicts the operation at -40°C . The results show a significant temperature variation, with the bags placed on the outer edge of the system at a relatively low temperature in comparison to the other bags. The increase in low temperature zones can be due to the introduction of a streamlined flow, allowing proper recirculation of air when it reaches the outer extremities of the system. As the operation continues to the set point of -70°C , there is an increasing amount of uniformity with temperature variations decreasing with each temperature increment. Fig. 18b and c shows

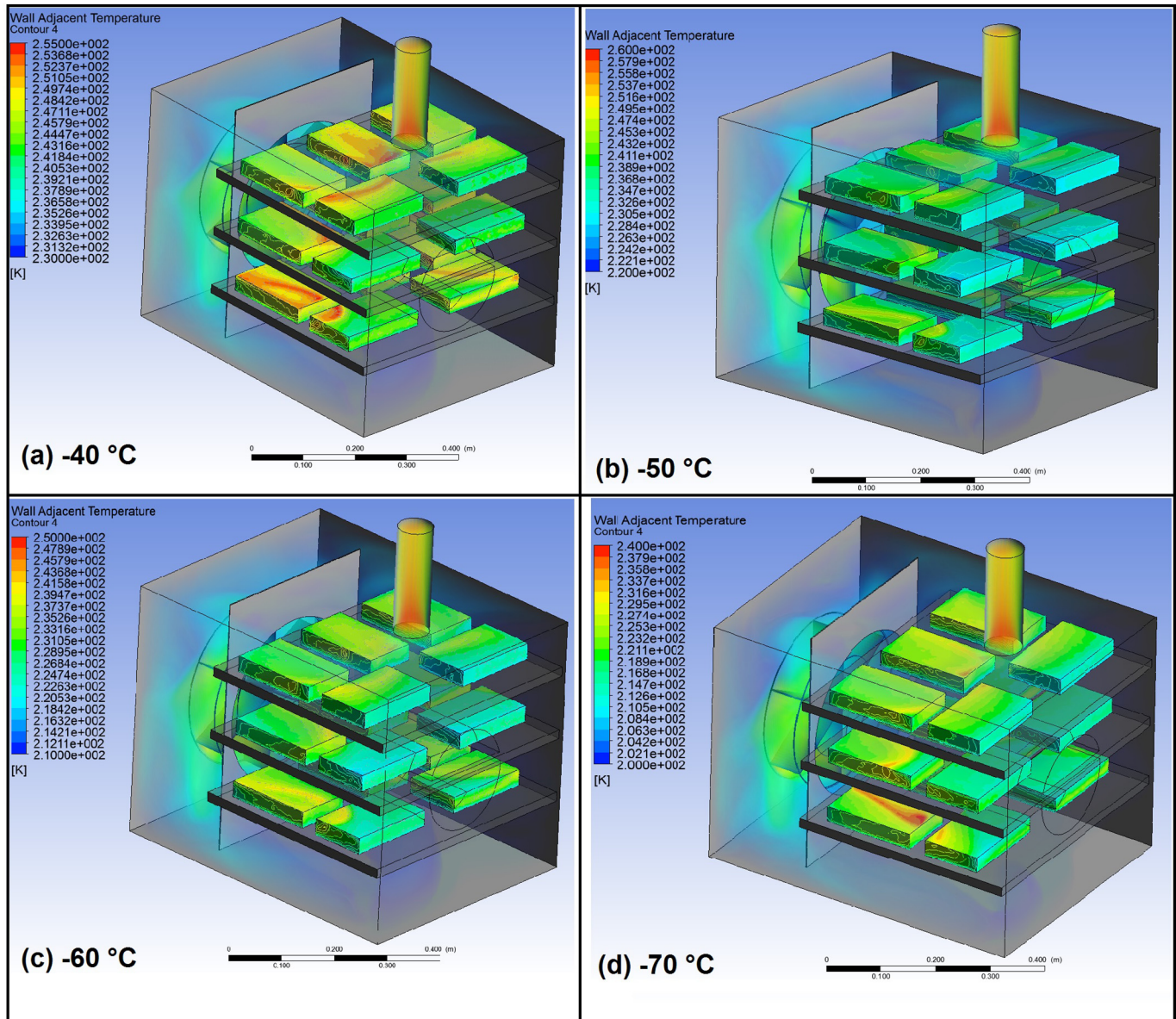


Fig. 20. Temperature contour plot of single stack at 285 RPM

the results for the operation at -50°C and -60°C , respectively, highlighting an increased uniformity. As observed in the original simulation, high temperature is observed on the bottom shelf towards the fan; the addition of another stack highlights a similar trend but stabilises towards the operation of the set point. The final operational set shows a small increase in temperature towards the exhaust, highlighting the pressure effects as expected but still displaying an overall uniformity.

6.2. Double stack at 1995 RPM

The double stack configuration was simulated again with a higher operation of 1995 RPM. Fig. 19a depicts the operation at -40°C , the contour plot shows a significant increase in temperatures which may be due to the increase in frictional forces between the gas and the glycerine-filled bag experienced with a higher RPM. The subsequent temperature plot in Fig. 19b shows an increased uniformity of the temperature, with a similar trend of low temperatures towards the back of the system. The temperature profile of the system highlights the increasing stability as the operation reaches the set point, with minimal levels of variation at the final set point.

6.3. Single stack at 285 RPM

The single stack configuration was simulated again under a lower RPM along the same temperature points as the original simulation. The results are shown in Fig. 20. The temperature contour plot at -40°C highlights a significant amount of high temperatures on the surface of the blood bags, indicating the frictional effects of the gas and the blood bags. The subsequent temperature plots reflect an increased stability as shown in Fig. 20. As the single stack system is identical to the original simulation, the increase in temperature experienced in Fig. 20 reflects areas previously identified as having recirculation and experiencing the suction effects of the exhaust. The operation of the fan throughout the configuration shows the slow reduction of high temperature areas, which still exist after reaching the set point. Similarly to the high RPM operation, the low RPM schematic depicts high temperature zones at the bottom shelf at the desired set point temperature. This can indicate poor flow circulation in the specific region in the bottom shelf.

7. Conclusions

It is evident from the results presented in this paper that the implementation of a liquid nitrogen injector improves the freezing performance of the system compared to direct immersion freezing, allowing achieving short freezing times without spikes in temperature. The lack of spiked temperatures highlights the lack of crystallisation within the product, leading to a higher product quality. In comparison to other freezing methods, the contact between product and liquid nitrogen is minimal. As observed from both CFD and experimental results, there are localised areas of extremely low temperatures; this may be due to the bag placement in relation to the liquid nitrogen injectors. The CFD data show a variation in temperature throughout each load but the temperature variation is still small in comparison to immersion freezing or other direct contact freezing methods. The freezing profile is also dependent on the positioning and stacking of the bags as reflected in the freezing predictions. It is evident that the addition of stacks increases the flow resistance throughout the system as the velocity increases. The results show that a double stack provides an excellent performance in a high RPM configuration, and could be implemented in systems where freezing is required in less than an

hour. Both high RPM sets of data showed an increased velocity resistance but produced the same temperature variations as their lower RPM counterpart, with the only difference being the decrease in freezing time experienced with a high RPM. The system itself achieves a low temperature smoothly and effectively without the need of additional systems to maintain the temperature, whilst maintaining product integrity with high levels of uniform product temperature.

Acknowledgements

This project was funded by AirProducts PLC (Agreement Number: 216-206-P).

References

- [1] Jouhara H, Olabi AG. Editorial: industrial waste heat recovery. *Energy* 2018;160:1–2. <https://doi.org/10.1016/j.ENERGY.2018.07.013>.
- [2] Olabi AG. Energy quadrilemma and the future of renewable energy. *Energy* 2016;108:1–6. <https://doi.org/10.1016/j.ENERGY.2016.07.145>.
- [3] Foley A, Olabi AG. Renewable energy technology developments, trends and policy implications that can underpin the drive for global climate change. *Renew Sustain Energy Rev* 2017;68:1112–4. <https://doi.org/10.1016/j.RSER.2016.12.065>.
- [4] Olabi AG. Renewable energy and energy storage systems. *Energy* 2017;136:1–6. <https://doi.org/10.1016/j.ENERGY.2017.07.054>.
- [5] Dima JB, Santos MV, Baron PJ, Califano A, Zaritzky NE. Experimental study and numerical modeling of the freezing process of marine products. *Food Bioprod Process* 2014;92:54–66. <https://doi.org/10.1016/j.fbp.2013.07.012>.
- [6] Biglia A, Comba L, Fabrizio E, Gay P, Aimonino DR. Case studies in food freezing at very low temperature. *Energy Proc* 2016;101:305–12. <https://doi.org/10.1016/j.egypro.2016.11.039>.
- [7] Kiani H, Sun D-W. Water crystallization and its importance to freezing of foods: a review. *Trends Food Sci Technol* 2011;22:407–26. <https://doi.org/10.1016/j.tifs.2011.04.011>.
- [8] Paciulli M, Ganino T, Pellegrini N, Rinaldi M, Zaupa M, Fabbri A, et al. Impact of the industrial freezing process on selected vegetables — Part I. Structure, texture and antioxidant capacity. *Food Res Int* 2015;74:329–37. <https://doi.org/10.1016/j.FOODRES.2014.04.019>.
- [9] Kondjoyan A. A review on surface heat and mass transfer coefficients during air chilling and storage of food products. *Int J Refrig* 2006;29:863–75. <https://doi.org/10.1016/j.ijrefrig.2006.02.005>.
- [10] Rooni V, Raud M, Kikas T. The freezing pre-treatment of lignocellulosic material: a cheap alternative for Nordic countries. *Energy* 2017;139:1–7. <https://doi.org/10.1016/j.ENERGY.2017.07.146>.
- [11] Han Y, Li M, Wang Y, Li G, Ma X, Wang R, et al. Impedance matching control strategy for a solar cooling system directly driven by distributed photovoltaics. *Energy* 2019;168:953–65. <https://doi.org/10.1016/j.ENERGY.2018.11.148>.
- [12] Edwin M, Joseph Sekhar S. Techno- Economic evaluation of milk chilling unit retrofitted with hybrid renewable energy system in coastal province. *Energy* 2018;151:66–78. <https://doi.org/10.1016/j.ENERGY.2018.03.050>.
- [13] Edwin M, Sekhar SJ. Thermal performance of milk chilling units in remote villages working with the combination of biomass, biogas and solar energies. *Energy* 2015;91:842–51. <https://doi.org/10.1016/j.ENERGY.2015.08.103>.
- [14] Reno MJ, Resende JV, Peres AP, Giarolla TMO, Prado MET. Heat transfer and energy consumption in the freezing of guava pulp in large containers. *Appl Therm Eng* 2011;31:545–55. <https://doi.org/10.1016/j.applthermaleng.2010.10.015>.
- [15] Becker BR, Fricke BA. Heat transfer coefficients for forced-air cooling and freezing of selected foods. *Int J Refrig* 2004;27:540–51. <https://doi.org/10.1016/j.ijrefrig.2004.02.006>.
- [16] Zhao CJ, Han JW, Yang XT, Qian JP, Fan BL. A review of computational fluid dynamics for forced-air cooling process. *Appl Energy* 2016;168:314–31. <https://doi.org/10.1016/j.apenergy.2016.01.101>.
- [17] Alvarez G, Bournet P-E, Flick D. Two-dimensional simulation of turbulent flow and transfer through stacked spheres. *Int J Heat Mass Tran* 2003;46:2459–69. [https://doi.org/10.1016/S0017-9310\(02\)00546-X](https://doi.org/10.1016/S0017-9310(02)00546-X).
- [18] Urquiola A, Alvarez G, Flick D. Frost formation modeling during the storage of frozen vegetables exposed to temperature fluctuations. *J Food Eng* 2017. <https://doi.org/10.1016/j.jfoodeng.2017.06.025>.
- [19] Hu Z, Sun D-W. Predicting local surface heat transfer coefficients by different turbulent $k-\epsilon$ models to simulate heat and moisture transfer during air-blast chilling. *Int J Refrig* 2001;24:702–17. [https://doi.org/10.1016/S0140-7007\(00\)00081-5](https://doi.org/10.1016/S0140-7007(00)00081-5).
- [20] Moerman F, Fikiin K. Chapter 20 – hygienic design of air-blast freezing systems. *Handb Hyg Contr Food Ind* 2016:271–316. <https://doi.org/10.1016/B978-0-08-100155-4.00020-0>.
- [21] Li D, Chen B, Wu WJ, Wang GX, He YL. Multi-scale modeling of tissue freezing during cryogen spray cooling with R134a, R407c and R404a. *Appl Therm Eng* 2014;73:1489–500. <https://doi.org/10.1016/j.applthermaleng.2014.03.034>.

- [22] Liang D, Lin F, Yang G, Yue X, Zhang Q, Zhang Z, et al. Advantages of immersion freezing for quality preservation of litchi fruit during frozen storage. *LWT - Food Sci Technol* 2015;60:948–56. <https://doi.org/10.1016/j.lwt.2014.10.034>.
- [23] Alberto Dopazo J, Fernández-Seara J. Experimental evaluation of freezing processes in horizontal plate freezers using CO₂ as refrigerant. *Int J Refrig* 2012;35:2093–101. <https://doi.org/10.1016/j.jrefrig.2012.08.018>.
- [24] Xin Y, Zhang M, Xu B, Adhikari B, Sun J. Research trends in selected blanching pretreatments and quick freezing technologies as applied in fruits and vegetables: a review. *Int J Refrig* 2015;57:11–25. <https://doi.org/10.1016/j.jrefrig.2015.04.015>.
- [25] Wang J, Yang X-H, Mujumdar AS, Wang D, Zhao J-H, Fang X-M, et al. Effects of various blanching methods on weight loss, enzymes inactivation, phytochemical contents, antioxidant capacity, ultrastructure and drying kinetics of red bell pepper (*Capsicum annuum* L.). *LWT* 2017;77:337–47. <https://doi.org/10.1016/j.lwt.2016.11.070>.
- [26] Jaworska G, Bernaś E. Effects of pre-treatment, freezing and frozen storage on the texture of *Boletus edulis* (Bull. Fr.) mushrooms. *Int J Refrig* 2010;33:877–85. <https://doi.org/10.1016/j.jrefrig.2009.12.031>.
- [27] Xiao H-W, Pan Z, Deng L-Z, El-Mashad HM, Yang X-H, Mujumdar AS, et al. Recent developments and trends in thermal blanching – a comprehensive review. *Inf Process Agric* 2017;4:101–27. <https://doi.org/10.1016/j.inpa.2017.02.001>.
- [28] Weng C-C, Lin M-C, Huang M-J. A waste cold recovery from the exhausted cryogenic nitrogen by using thermoelectric power generator. *Energy* 2016;103:385–96. <https://doi.org/10.1016/j.energy.2016.02.146>.
- [29] Zhao Y, Wang S, Li Y. Thermoelectric power generation using LNG cold energy and flue gas heat. *Energy Proc* 2017;105:1932–5. <https://doi.org/10.1016/j.egypro.2017.03.562>.
- [30] Ghorbani B, Hamed M-H, Amidpour M, Mehrpooya M. Cascade refrigeration systems in integrated cryogenic natural gas process (natural gas liquids (NGL), liquefied natural gas (LNG) and nitrogen rejection unit (NRU)). *Energy* 2016;115:88–106. <https://doi.org/10.1016/j.energy.2016.09.005>.
- [31] Gurruchaga H, Saenz del Burgo L, Hernandez R, Orive G, Selden C, Fuller B, et al. Advances in the slow freezing cryopreservation of microencapsulated cells. *J Contr Release* 2018;281:119–38. <https://doi.org/10.1016/j.jconrel.2018.05.016>.
- [32] Ahmad A, Al-Dadah R, Mahmoud S. CFD modelling of a novel liquid Nitrogen/Air engine and cryogenic heat exchanger for small scale applications. *Energy Proc* 2017;142:3654–60. <https://doi.org/10.1016/j.egypro.2017.12.258>.
- [33] Espinoza Rodezno LA, Sundararajan S, Solval KM, Chotiko A, Li J, Zhang J, et al. Cryogenic and air blast freezing techniques and their effect on the quality of catfish fillets. *LWT - Food Sci Technol* 2013;54:377–82. <https://doi.org/10.1016/j.lwt.2013.07.005>.
- [34] Hu Z, Sun D. Effect of fluctuation in inlet airflow temperature on CFD simulation of air-blast chilling process. *J Food Eng* 2001;48:311–6. [https://doi.org/10.1016/S0260-8774\(00\)00172-2](https://doi.org/10.1016/S0260-8774(00)00172-2).
- [35] Issa RJ, Lawrence T. Experimental heat transfer study of beef carcasses chilled by mist sprays. *Exp Heat Transf* 2014;28:69–88. <https://doi.org/10.1080/08916152.2013.813877>.
- [36] Dempsey P, Bansal P. The art of air blast freezing: design and efficiency considerations. *Appl Therm Eng* 2012;41:71–83. <https://doi.org/10.1016/j.applthermaleng.2011.12.013>.
- [37] Góral D, Kluzka F. Heat transfer coefficient in impingement fluidization freezing of vegetables and its prediction. *Int J Refrig* 2012;35:871–9. <https://doi.org/10.1016/j.jrefrig.2011.11.010>.
- [38] Amarante A, Lanouisellé J-L. Heat transfer coefficients measurement in industrial freezing equipment by using heat flux sensors. *J Food Eng* 2005;66:377–86. <https://doi.org/10.1016/j.jfoodeng.2004.04.004>.
- [39] Amarante A, Lanouisellé J-L, Ramirez A. Direct measurement of heat transfer rates and coefficients in freezing processes by the use of heat flux sensors. *Chem Eng Res Des* 2003;81:1105–12. <https://doi.org/10.1205/026387603770866254>.
- [40] Fricke BA, Becker BR. Sensitivity of freezing time estimation methods to heat transfer coefficient error. *Appl Therm Eng* 2006;26:350–62. <https://doi.org/10.1016/j.applthermaleng.2005.07.005>.
- [41] Meziani S, Ioannou I, Jasniewski J, Belhaj N, Muller J-M, Ghoul M, et al. Effects of freezing treatments on the fermentative activity and gluten network integrity of sweet dough. *LWT - Food Sci Technol* 2012;46:118–26. <https://doi.org/10.1016/j.lwt.2011.10.017>.
- [42] Volkert M, Ananta E, Luscher C, Knorr D. Effect of air freezing, spray freezing, and pressure shift freezing on membrane integrity and viability of *Lactobacillus rhamnosus* GG. *J Food Eng* 2008;87:532–40. <https://doi.org/10.1016/j.jfoodeng.2008.01.008>.
- [43] Ketata M, Desjardins Y, Ratti C. Effect of liquid nitrogen pretreatments on osmotic dehydration of blueberries. *J Food Eng* 2013;116:202–12. <https://doi.org/10.1016/j.jfoodeng.2012.10.035>.
- [44] Agnelli ME, Mascheroni RH. Cryomechanical freezing. A model for the heat transfer process. *J Food Eng* 2001;47:263–70. [https://doi.org/10.1016/S0260-8774\(00\)00126-6](https://doi.org/10.1016/S0260-8774(00)00126-6).
- [45] Delgado AE, Sun D-W. Heat and mass transfer models for predicting freezing processes – a review. *J Food Eng* 2001;47:157–74. [https://doi.org/10.1016/S0260-8774\(00\)00112-6](https://doi.org/10.1016/S0260-8774(00)00112-6).
- [46] Gazda W. Application possibilities of the strategies of the air blast-cryogenic cooling process. *Energy* 2013;62:113–9. <https://doi.org/10.1016/j.energy.2013.06.054>.
- [47] Xu Z, Guo Y, Ding S, An K, Wang Z. Freezing by immersion in liquid CO₂ at variable pressure: response surface analysis of the application to carrot slices freezing. *Innovat Food Sci Emerg Technol* 2014;22:167–74. <https://doi.org/10.1016/j.ifset.2013.06.005>.
- [48] Awonorin SO. Analysis of the heat transfer coefficient for liquid nitrogen droplets in cryogenic freezing of foods: analyse du coefficient de transfert de chaleur de gouttelettes d'azote liquide dans des conditions de cryocongélation des aliments. *Int J Refrig* 1993;16:143–51. [https://doi.org/10.1016/0140-7007\(93\)90071-F](https://doi.org/10.1016/0140-7007(93)90071-F).
- [49] Lucas T, Flick D, Raoult-Wack AL. Mass and thermal behaviour of the food surface during immersion freezing. *J Food Eng* 1999;41:23–32. [https://doi.org/10.1016/S0260-8774\(99\)00068-0](https://doi.org/10.1016/S0260-8774(99)00068-0).
- [50] Sun Q, Sun F, Xia X, Xu H, Kong B. The comparison of ultrasound-assisted immersion freezing, air freezing and immersion freezing on the muscle quality and physicochemical properties of common carp (*Cyprinus carpio*) during freezing storage. *Ultrason Sonochem* 2018. <https://doi.org/10.1016/j.ultrasonch.2018.10.006>.
- [51] Radchenko NI. On reducing the size of liquid separators for injector circulation plate freezers. *Int J Refrig* 1985;8:267–9. [https://doi.org/10.1016/0140-7007\(85\)90004-0](https://doi.org/10.1016/0140-7007(85)90004-0).
- [52] Visser K. Automatic plate freezer development. *Int J Refrig* 1986;9:367. [https://doi.org/10.1016/0140-7007\(86\)90010-1](https://doi.org/10.1016/0140-7007(86)90010-1).
- [53] Cao XC, Wan JQ, Song LY. Experimental study of plate freezer with the ejector. *Proc Eng* 2015;121:1238–44. <https://doi.org/10.1016/j.proeng.2015.09.151>.
- [54] Estrada-Flores S. Cryogenic freezing of food. *Ref Modul Food Sci* 2016. <https://doi.org/10.1016/B978-0-08-100596-5.03175-9>.
- [55] Eggerstedt SN, Dietzel M, Sommerfeld M, Süverkrüp R, Lamprecht A. Protein spheres prepared by drop jet freeze drying. *Int J Pharm* 2012;438:160–6. <https://doi.org/10.1016/j.ijpharm.2012.08.035>.
- [56] Barresi AA, Marchisio DL. Computational Fluid Dynamics data for improving freeze-dryers design. *Data Br* 2018;19:1181–213. <https://doi.org/10.1016/j.dib.2018.05.141>.
- [57] Moerman F, Fikiin K. Hygienic design of air-blast freezing systems. *Elsevier*; 2016. p. 271–316. <https://doi.org/10.1016/B978-0-08-100155-4.00020-0>.
- [58] MacLeod CS, McKittrick JA, Hindmarsh JP, Johns ML, Wilson DI. Fundamentals of spray freezing of instant coffee. *J Food Eng* 2006;74:451–61. <https://doi.org/10.1016/j.jfoodeng.2005.03.034>.
- [59] Somasundaram S, Tay AAO. A study of intermittent liquid nitrogen sprays. *Appl Therm Eng* 2014;69:199–207. <https://doi.org/10.1016/j.applthermaleng.2013.11.066>.
- [60] Huan Z, He S, Ma Y. Numerical simulation and analysis for quick-frozen food processing. *J Food Eng* 2003;60:267–73. [https://doi.org/10.1016/S0260-8774\(03\)00047-5](https://doi.org/10.1016/S0260-8774(03)00047-5).
- [61] Alhamdan A, Hassan B, Alkahtani H, Abdelkarim D, Younis M. Freezing of fresh Barhi dates for quality preservation during frozen storage. *Saudi J Biol Sci* 2018;25:1552–61. <https://doi.org/10.1016/j.sjbs.2016.02.003>.
- [62] Oswald I, Rickert M, Brüggemann G-P, Niehoff A, Fonseca Ulloa CA, Jahnke A. The influence of cryopreservation and quick-freezing on the mechanical properties of tendons. *J Biomech* 2017;64:226–30. <https://doi.org/10.1016/j.jbiomech.2017.08.018>.
- [63] Akisaka T, Yoshida H, Hosoi M. Improved preservation of *Amoeba proteus* ultrastructure revealed by quick-freezing followed by freeze-substitution. *Eur J Protistol* 2000;36:303–15. [https://doi.org/10.1016/S0932-4739\(00\)80006-1](https://doi.org/10.1016/S0932-4739(00)80006-1).
- [64] Bulut M, Bayer Ö, Kırtıl E, Bayındırlı A. Effect of freezing rate and storage on the texture and quality parameters of strawberry and green bean frozen in home type freezer. *Int J Refrig* 2018;88:360–9. <https://doi.org/10.1016/j.jrefrig.2018.02.030>.
- [65] De Santis L, Cotichio G. Reprint of: theoretical and experimental basis of slow freezing. *Reprod Biomed Online* 2011;23:290–7. <https://doi.org/10.1016/j.rbmo.2011.07.001>.
- [66] Bansal P, Fothergill D, Fernandes R. Thermal analysis of the defrost cycle in a domestic freezer. *Int J Refrig* 2010;33:589–99. <https://doi.org/10.1016/j.jrefrig.2009.11.012>.
- [67] Năstase G, Lyu C, Ukpai G, Şerban A, Rubinsky B. Isochoric and isobaric freezing of fish muscle. *Biochem Biophys Res Commun* 2017;485:279–83. <https://doi.org/10.1016/j.bbrc.2017.02.091>.
- [68] Năstase G, Perez PA, Şerban A, Dobrovicescu A, Ştefănescu M-F, Rubinsky B. Advantages of isochoric freezing for food preservation: a preliminary analysis. *Int Commun Heat Mass Tran* 2016;78:95–100. <https://doi.org/10.1016/j.jcheatmasstransfer.2016.08.026>.
- [69] Rubinsky B, Perez PA, Carlson ME. The thermodynamic principles of isochoric cryopreservation. *Cryobiology* 2005;50:121–38. <https://doi.org/10.1016/j.cryobiol.2004.12.002>.
- [70] Szobota SA, Rubinsky B. Analysis of isochoric subcooling. *Cryobiology* 2006;53:139–42. <https://doi.org/10.1016/j.cryobiol.2006.04.001>.
- [71] Bilbao-Sainz C, Sinrod A, Powell-Palm M, Dao L, Takeoka G, Williams T, et al. Preservation of sweet cherry by isochoric (constant volume) freezing. *Innovat Food Sci Emerg Technol* 2018. <https://doi.org/10.1016/j.ifset.2018.10.016>.
- [72] Jouhara H, Chauhan A, Nannou T, Almahmoud S, Delpech B, Wrobel LC. Heat pipe based systems - advances and applications. *Energy* 2017;128:729–54. <https://doi.org/10.1016/j.energy.2017.04.028>.
- [73] Functions AFU. *Ansys Fluent Guide* 2011:1–39.